Journal Pre-proof

Neutrosophic Entropy-based ingenious measurement for Fast Fourier Transforms based classification of process-parameters and wear resistance of Friction-Stir processed hybrid AA7075- B_4C Aluminium metal-matrix composites

Rajeev Kumar, Jujhar Singh, Shubham Sharma, Changhe Li, Grzegorz Królczyk, Szymon Wojciechowski

PII: S2238-7854(22)01065-1

DOI: https://doi.org/10.1016/j.jmrt.2022.07.026

Reference: JMRTEC 5260

To appear in: *Journal of Materials Research and Technology*

Received Date: 8 May 2022

Revised Date: 2 July 2022

Accepted Date: 5 July 2022

Please cite this article as: Kumar R, Singh J, Sharma S, Li C, Królczyk G, Wojciechowski S, Neutrosophic Entropy-based ingenious measurement for Fast Fourier Transforms based classification of process-parameters and wear resistance of Friction-Stir processed hybrid AA7075- B_4C Aluminium metal-matrix composites, *Journal of Materials Research and Technology*, https://doi.org/10.1016/j.jmrt.2022.07.026.

Neutrosophic Entropy-based ingenious measurement for Fast Fourier Transforms based classification of process-parameters and wear resistance of Friction-Stir processed hybrid AA7075- B_4C Aluminium metal-matrix composites

Rajeev Kumar[1, 2], Jujhar Singh[3], Shubham Sharma[4,5*], Changhe Li[6], Grzegorz Królczyk[7*], Szymon Wojciechowski[8*]

[1]School of Mechanical Engineering, Lovely Professional University, Phagwara-144411, India. E-Mail: rajeev14584@lpu.co.in (RK).

[2]Research Scholar, Department of Mechanical Engg., IK Gujral Punjab Technical University, Main campus, Kapurthala-144603, India. E-Mail: rajeev14584@lpu.co.in (RK)

[3]Department of Mechanical Engineering, IK Gujral Punjab Technical University, Kapurthala, Punjab, India. Email: jujharsingh2085@gmail.com (JS)

[4]Department of Mechanical Engineering, Indian Institute of Technology, IIT-Ropar, 140001, Rupnagar, Punjab, India. Email: shubham543sharma@gmail.com, shubhamsharmacsirclri@gmail.com (SS)

[5]Univesity Centre for Research and Development, Chandigarh University, Mohali, India. E-Mail: shubham543sharma@gmail.com, shubhamsharmacsirclri@gmail.com (SS)

[6]School of Mechanical and Automotive Engineering, Qingdao University of Technology, 266520, Qingdao, China. E-Mail: sy_lichanghe@163.com (CL)

[7]Department of Manufacturing and Materials Engineering, Faculty of Mechanical Engineering, Opole University of Technology, Mikolajczyka 5, 45-271 Opole, Poland. E-Mail: g.krolczyk@po.opole.pl (GK)

[8]Faculty of Mechanical Engineering and Management, Poznan University of Technology, Poznan, 60-965, Poland. E-Mail: sjwojciechowski@o2.pl (SW)

***Correspondence:** sjwojciechowski@o2.pl (SW); shubham543sharma@gmail.com; shubhamsharmacsirclri@gmail.com (SS); g.krolczyk@po.opole.pl (GK)

Abstract: The underlying study propounds novel hyperbolic fuzzy entropy (HFE) and single valued neutrosophic entropy (NFE) based methodology for classifying the processing parameters employed for studying the wear-resistance of friction-stir-processing (FSP) of AA7075 aluminum, allow incorporated with B_4C particles under different reinforcement conditions. Fast Fourier transform (FFT) was applied for the acquisition of vibration data. An alloy sheet with a thickness of 5mm and dimensions $180\times160\times5$ was machined on the aluminium plates for the purpose of accommodating B_4C particles. The experiments were

performed at varying tool rotational speeds (1400rpm, 1500rpm and 1600rpm) , feed rate (30mm/min, 40mm/min and 50mm/min) with plunge depth and constant tilt angles of 3.14°. After acquitting vibration data through FFT, the lower and upper bounds from energy eigenvalues of each processing parameters were extracted and thereafter rehabilitated into the forms of non-probabilistic sets, also called fuzzy sets (FSs) and single-valued neutrosophic sets (SVNSs) consecutively. The tool rotational speed of 1600rpm with feed rate 30mm/min was found to be the most superlative processing parameter owing to its maximum HFE and NFE values respectively. The wear-properties of the fabricated-samples were investigated employing pin-on tribometer. The investigations made in this study reveal that the fabricated specimen with tool rotational-speed 1600 rpm and feed-rate 30 mm/min was having higher wear resistance and coefficient-of-friction (COF). The proposed entropy-based method of classification of processing parameters can help the readers to improve surface integrity and enhancement of mechanical & chemical properties of the selected aluminium alloy as well as other related metal composites.

Keywords: Fuzzy Entropy, Neutrosophic Entropy, FSP, Fast Fourier, Feed-Rate, Rotational Speed.

1 Introduction

Using a "solid-state-processing-technique" named FSP, which operates on the theory of Friction-Stir-Welding (FSW), a SCL with a fine-grained-microstructure can be produced **[1]**. The FSP physically mixes two or more materials consistently, improves the material's tribological and mechanical qualities. **[2]**. AA-7075 is the most extensively used material for aerospace and automotive applications **[3]**. A.Shafiei-Zarghani et al. **[4]** investigated the effect of the passes number on the grain size and mechanical properties of a composite fabricated by inserting nano Al_2O_3 particles in an 'aluminium-alloy-substrate' which use FSP to substrate an Al/Al_2O_3 nano-SCL. Al_2O_3 particles were wrapped in 5 and 4 mm wide and depth groove, made respectively on the Al alloy-substratum, and subjected to passes count as one-to-four. The particles of the Al_2O_3 were dispersed evenly with the elevated number of FSP passes. A study on the basis of different FSP parameters by Barmouz et al. **[5]** and tested the microstructural behaviour and mechanical-properties of Cu/SiC MMC. The microstructure result shows that the grain-size of base metal is about 40-50 µm and grain size of samples fabricated without SiC particles was reduced from about 9.5 µm to 5.3 µm with

increasing feed rate of 40, 80 and 200 mm/min. Ali dokht et al. **[6]** fabricated a surface hybrid-composites by assorting MoS_2 and SiC particles by using FSP. The result show that the average size of as-received particles was 30 µm which was reduced to 10 µm due to homogeneous distribution of MoS_2 and SiC particles. The hardness result presented that the processed A356 alloy has high hardness in comparison to that of as received A356 alloy. The effect of ultrasonic vibration on the microhardness, tensile-strength, temperature and downward force on the specimen of Al6061 – T6 aluminium alloy was investigated Amini et al **[7]** and presented that the microhardness of the 'base-alloy' was 82-HV, which was enhanced to about 15% in advancing path there was no any drastic change in retreating path measured at a 'tool-speed' of 1000 rpm and traverse-speeds of 100 and 142 mm/min. The results show that the ultimate-tensile-strength of base alloy was 309 MPa, and the specimen fabricated by ultrasonic-vibrations have increased strength of about 10%. The implementation of ultrasonic vibration reduces the 'downward-force' to about 25% and welding-force to about 10%. The result presented that the temperature increases by addition of 'ultrasonic-vibration' in FSW. the effect of 'ultrasonic-vibration' on the tensile-strength, microhardness and grain size of the 2024-aluminium alloy welded by FSW and compared with that of without ultrasonic vibrations. The result presented that the 'mean-grain-size' of base metal was around 43.05 µm reduced to 3.37 µm after FSW in the stir zone and on application of ultrasonic vibration it was 3.47 µm. the microhardness result shows that base metal, FSW and UaFSW has a hardness of 31.6 HV,52.9 HV and 55.4 HV respectively. The tensile-strength of the base metal was 430.85 MPa and that of FSW and UaFSW was 103.25 MPa and 156.31 MPa respectively. Due to better stirring effect the cross-section area of macro-pores get reduced in UaFSW and presented well by Eliseev et al. **[8]**. Hybrid and Mono SCL of 'Al-matrix (Al5083)' consisting TiC and B_4C was made by FSP and reported by N. Yuvaraj et al **[9]** on further investigation of tribological and mechanical properties 4 FSP passes made on the SCL were carried out. The results show that the FSPed specimen has a higher 'hardness' and 'strength' value compared with the base alloy being uniform-dissemination of the ceramic particles. Deva raju et al. **[10]** made with the addition of'Gr+SiC' and 'Al_2O_3+SiC' particles of average size of 20 µm on 6061-T6 Al plate by using FSP. The mixture of reinforcement particles was added to the groove by volume-ratio of 4% and 8%, respectively. The processing parameters were set to 900 rpm 'rotational-speed', and 40 mm/min 'traverse-speed'. The microstructure results show that the reinforcement particles get uniformly-dispersed within the 'nugget-zone' and the size of the 'reinforcement-particles' gets reduced. The microhardness value of Al-SiC/Al_2O_3 and Al-SiC/Gr was 120 HV and 108

HV respectively which was greater in comparison with as-received base alloy of 104 HV due to the existence of hard-particles. The Al-SiC/Gr specimen shows lower COF and increased wear-resistance in comparison with the Al-SiC /Al_2O_3 due to creation of Gr layer which exhibits as a further solid-lubricant **[11-14]**. Sathiskumar et al **[15-16]** has identified Cu/B_4C MMC by incorporating B_4C particles in the groove of the plate of different volume fractions (0, 6, 12, 18 and 24) and investigated the wear and microstructural behaviour of the sample. The result presented that at 0 vol% and 24 vol% the area of the composite was 44 mm^2 and 24 mm^2 respectively. They also produced a CMC reinforced with a variety of reinforcing-particles such as B_4C, TiC, SiC, Al_2O_3 and WC. The role of FSP parameters such as the 'SCL field', 'wear-rate' and 'microhardness' on the characteristics of copper-surface-composites was investigated adopting empirical relationships. The parameters were groove width, kind of ceramic particle, 'tool-rotating speed', and 'traverse-speed'. The microstructural characterisation of manufactured surface composites was accounted for using the analytical equations created to examine the impact of these parameters on CMC characteristics. The surface composite made by reinforcing B_4C particles has low wear-rate and high microhardness. Rajwinder Singh Gill et al. [17] Aluminum metal matrix composites (Al-MMCs) are incredibly strong and lightweight, have high strength-to-weight ratios, and have several uses in the construction, marine, aerospace, defence, and automotive industries. To improve their mechanical and frictional behaviour, these materials can be reinforced with ceramic materials in a variety of ways. The most often utilised reinforcing materials are alumina, silicon carbide, boron carbide, and aluminium oxide. Numerous research communities have demonstrated that different reinforcements have distinctive impacts on aluminium composites. In this work, the impact of various reinforcements on the tribological characteristics of Al-MMCs are reviewed. The mechanical and microstructural properties and of Cu sheets fabricated by incorporating 25 µm SiC particles using FSP was presented by Akramifard et al. **[18]** The result shows that the FSPed specimen have 'fine and equiaxed-grain' in the stir-zone due to the even-distribution of SiC particles in the metal matrix. The wear rate of the pure Cu (4.24×10^{-5} gr/m) was reduced in comparison with Cu/SiC composite (1.92×10^{-5} gr/m). The mean coefficient of friction of Cu/SiC composites and pure Cu are 0.52 and 0.45 respectively. The hardness value and wear behaviour of Cu/SiC composite was better from pure Cu. In FSP, when the tool is inserted inside the workpiece it exerts certain force perpendicular to the length of the workpiece. This force creates certain vibration in the workpiece the analyses of these vibrations is becoming important task to predict the prominent parameters for processing. For measuring the vibrations of the system

their various ways but we have to concern the temperature change during the process because at higher temperature some vibration measurement system losses their accuracy. Therefore, it is required to select the vibration system according to the context of FSP and these vibration leads to certain outcome on the mechanical-properties of the fabricated material. Many researchers, investigated the effect of vibration on the properties of the workpiece and presented that with increasing randomness in the vibration signal the processing losses its accuracy and leads to reduce the various properties of the material. That`s why the analysis of these vibrations should carry out so that we can judge the changes in the material-properties and conclude the suitable processing parameters.

Due of its broad features, such as good 'corrosion-resistance' and 'fatigue-strength', AA7075 is most extensively used material. AA 7075 alloy has a compactness of 2.81 gm/cm^3. In comparison to many steels, strength of these alloys is higher. The usage of AA 7075 is restricted because to its expensive cost [3]. The nominal composition of the Al 7075 is shown in Table 1.

Table 1. Composition of alloy; AA7075 (wt%)

Zn	Mg	Cr	Cu	Al
5.60	2.50	0.23	1.60	Bal.

Recently, Ikumanpayi and Akinlabi **[19]** employed root mean square (RMS) for the construction process parameters and deployed them for reckoning the optimal FST for AA7075-T651 alloy. However, the statistical root mean square measure behaves insignificantly under short bursts of vibration signal with low intensity and hence may not be capable for improving the surface integrity of aluminium metal composites. Fuzzy set theory propounded by Zadeh **[20]** can play an eminent role for the enhancement of surface modification techniques under varying reinforcement conditions. However, the fuzzy sets, since its invention, have been rehabilitated into a number of variants including intuitionistic 'fuzzy-sets', single-valued neutrosophic-sets, interval-valued intuitionistic 'fuzzy-sets' **[21]** and so on. Unfortunately, the existing FSP techniques for enhancing the mechanical properties of metal composites have been found deprived of utilizing FS (fuzzy set) and NS (neutrosophic set) theory. However, the NS theory **[21]** can play a smart role in optimizing the FST parameters. However, the enduring 'neutrosophic-set' theory mainly deals with its

'theoretical aspects', but it does not include vibrational problems which demand analysis of surface-roughness, surface-topography, wear-resistance, microstructural analysis, etc. Moslem Paidar et al. [22] discussed how the fabrication of 10 cycle-accumulative roll-bonded Al-2 percent B4C composites affected the microstructure, mechanical, wear, and fracture characteristics. The Al-2%B_4C composite's microhardness, tensile strength (86.84-173.92 MPa), and fracture resilience all saw direct improvements as the number of tool-passes increased. An increase in tool passes improves the composite's tribological characteristics. As the number of tool passes was changed from 1 to 8, the wear rate, upper bounds, and mid-fluctuation lines of the friction coefficient fell from $6.198X10^{-5}$ to $1.095X10^{-5}$ mm3/Nm, 0.56 to 0.19, and 0.31 to 0.11, respectively. Alireza Moradi Faradonbeh et al. [23] Friction stir welding (FSW) of an Al-B_4C composite produced by accumulative roll bonding over ten cycles was carried out. Four distinct pin geometries (cylindrical, square, triangular, and hexagonal) were chosen in order to examine the effects of pin geometry on microstructure and mechanical properties. It was discovered that the FSW settings significantly influenced the distribution and fragmentation of reinforcement particles in the stir zone. The dispersion of B_4C particles in the aluminum matrix eventually became uniform as the tool travel speed rose. It was found that tool travel speed had a less impact on peak temperature than tool rotational speed did. The results of the tensile properties and microhardness tests revealed a bilateral relationship between the tensile strength and the tool travel speed. Moslem Paidar et al. [24] The performance of the as-cast Mg- B_4C composites is hampered by the large and irregular particle sizes of B_4C in the Mg matrix. To combat this, the as-cast Mg-10% B_4C composite underwent secondary solid-state friction stir processing using a flow-enhancing double-pin tool, and the resulting outcome was compared with that of a single-pin tool. Investigations and comparisons were made regarding the treated composites' microstructure, hardness, tensile strength, wear, and shattered surface. The double-pin tool's additional pin-shearing effect and complicated pin-induced interactive material flow lead to greater B_4C particle refinement in the Mg-10% B_4C composite. To meet this exigency and to reckon the quality of processed material under a fuzzy and neutrosophic environment, an effort has been gained in this direction by establishing new hyperbolic fuzzy entropy (HFE) and single-valued neutrosophic entropy (HNE) measures and then applying them for classifying the underlying processing parameters and studying the wear resistance of FSP AA7075 aluminum allow incorporated with B_4C particles. The projected fuzzy and neutrosophic entropy measures are superior and efficacious over the enduring Deluca & Termini fuzzy entropy measure which may exhibit indeterminacy and inconsistency in the evaluation

analysis. Thus, in the research work, the specific wear rate under dry conditions and vibrational analysis was carried out by using novel hyperbolic fuzzy-entropy (HFE) and single-valued neutrosophic-entropy (NFE) based methodology. The Fast-Fourier Transform (FFT) of the vibration signal was generated for analyzing the dispersion and peaks in the signal. Furthermore, analysis of the signal was carried out by using some statistical parameters such as Standard Deviation, Kurtosis and Shannon to investigate the randomness in the signal at different processing parameters.

The remaining part of the proposed research work is as given.

Section 2.1 deals with the opening of basic pre-requisites required for understanding the proposed study whereas **Section 2.2** is devoted to the establishment of a novel hyperbolic-fuzzy entropy amount hinged on a fuzzy set followed by a novel-symmetric hyperbolic fuzzy-cross-entropy (symmetric discrimination information) measure hinged on two fuzzy-sets. **Section 2.3** establishes another novel hyperbolic single-valued neutrosophic-entropy measure hinged on a single valued neutrosophic-set. **Section 3 describes entropy-based methodology for FSP process parameters and rest other sections or sub-sections has been detailed shown in fig.1,**

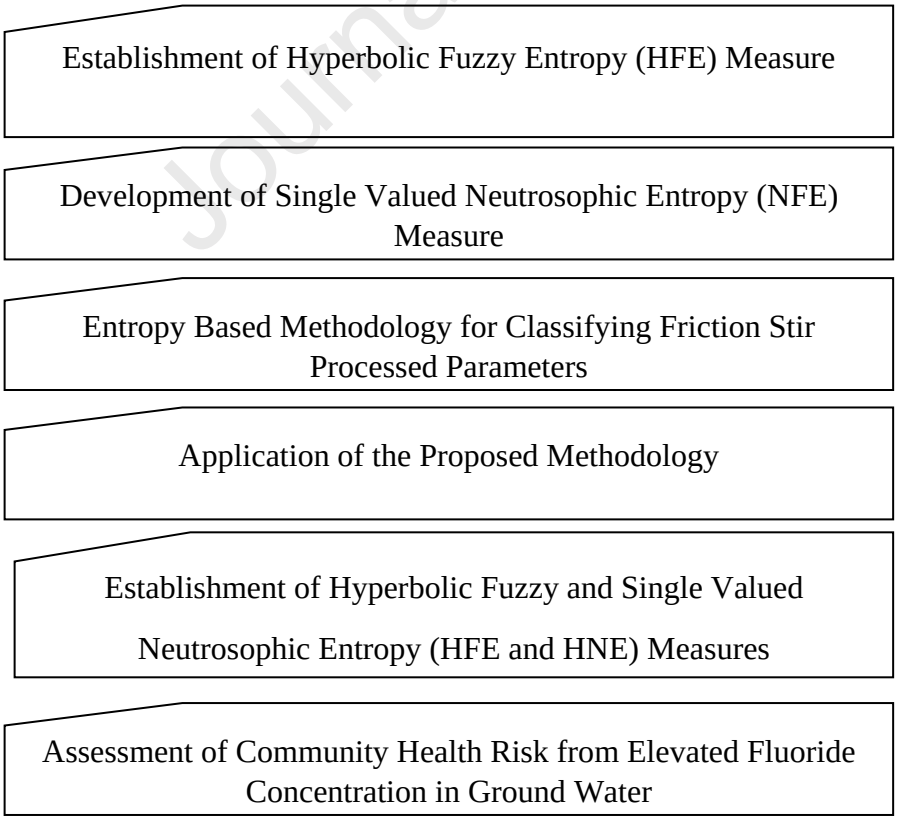

Fig.1: Research-Methodology of the work.

2. Experimentations:

2.1. Underlying Theories and Preliminaries

The section provides a greater knowledge of the core principles of information theory, which is necessary for the study's continuing progress.

Def. 2.1. Fuzzy Set (FS): A 'fuzzy-set' P_{FS}^{a} in a 'finite-discourse' of universe $U=\left(x_1,x_2,...,x_n\right)$ is an entity of the form: $P_{FS}^{a}=\left(<x_i,\mu_{P^a}\left(x_i\right)>|\,x_i\in U\right)$ where $\mu_{P^a}\left(x_i\right):U\in\left[0,1\right]$ represents membership function and satisfies $0\le\mu_{P^a}(x_i)\le 1$. Also, the complement $C\left(P_{FS}^{a}\right)$ of the fuzzy set $P_{FS}^{a}\in U$ is an object represented by $C\left(P_{FS}^{a}\right)=\left(x_i,1-\mu_{P^a}(x_i)>|\,x_i\in U\right)$.

Def. 2.2. Fuzzy-Entropy: If $F(U)$ exhibits the collection of all fuzzy-sets in U and $P_{FS}^{a}=\left(<x_i,\mu_{P^a}\left(x_i\right)>|\,x_i\in U\right)$ be any fuzzy set. Then a function $H_{FS}:F\left(U\right)\to R^{+}$ (the set of non-negative reals) is called as 'fuzzy-entropy-measure' if it satisfies the following conditions

$(i)\,H_{FS}\left(P_{FS}^{a}\right)\ge 0\forall P_{FS}^{a}\in F\left(U\right)$ with equality if $\mu_{P^a}\left(x_i\right)=0$ or 1. (ii) $H_{FS}\left(P_{FS}^{a}\right)$ does not change whenever $\mu_{P^a}\left(x_i\right)$ is replaced by its counterpart $1-\mu_{P^a}\left(x_i\right)$ (iii) $H_{FS}\left(P_{FS}^{a}\right)$ is a concave function of $\mu_{P^a}\left(x_i\right)$. In other words, $\dfrac{\partial^2 H_{FS}\left(P_{FS}^{a}\right)}{\partial\mu_{P^a}^{2}\left(x_i\right)}<0\forall\mu_{P^a}\left(x_i\right)\in\left[0,1\right]$. (iv) Because of concavity, $H_{FS}\left(P_{FS}^{a}\right)$ should possess its maximum value which arises at $\mu_{P^a}(x_i)=\dfrac{1}{2}$.

Def.2.3: Symmetric Fuzzy-Cross-Entropy

Let $P_{FS}^{a}=\left(<x_i,\mu_{P^a}\left(x_i\right)>|\,x_i\in U\right)$ and $Q_{FS}^{a}=\left(<x_i,\mu_{Q^a}\left(x_i\right)>|\,x_i\in U\right)$ are any two 'fuzzy-sets' in $U=\left(x_1,x_2,...,x_n\right)$ which are quantified by their 'truth-membership-functions' $\mu_{P^a}\left(x_i\right),\mu_{Q^a}\left(x_i\right):U\to\left[0,1\right]$ with the condition $0\le\mu_{P^a}\left(x_i\right),\mu_{Q^a}\left(x_i\right)\le 1$. Then, a function $H_{CE}:F\left(U\right)\times F\left(U\right)\to R^{+}$ is called as symmetric fuzzy cross-entropy or symmetric

discrimination information measure hinged on two fuzzy-sets P_{FS}^{a} and Q_{FS}^{a} if $(i)\, H_{CE}\left(P_{FS}^{a}, Q_{FS}^{a}\right) \geq 0 \forall P_{FS}^{a}, Q_{FS}^{a} \in F(U)$ and equality occurs when $P_{FS}^{a} = Q_{FS}^{a}$.

$(ii)\, H_{CE}\left(P_{FS}^{a}, Q_{FS}^{a}\right) = H_{CE}\left(Q_{FS}^{a}, P_{FS}^{a}\right)$. In other words, $H_{CE}\left(P_{FS}^{a}, Q_{FS}^{a}\right)$ is symmetric in nature.

$(iii)\, H_{CE}\left(C\left(P_{FS}^{a}\right), C\left(Q_{FS}^{a}\right)\right) = H_{CE}\left(P_{FS}^{a}, Q_{FS}^{a}\right)$ which means $H_{CE}\left(P_{FS}^{a}, Q_{FS}^{a}\right)$ does not change whenever $\mu_{P^a}(x_i), \mu_{Q^a}(x_i) : U \to [0,1]$ are replaced by consecutively

Def. 2.4: Single-Valued-Neutrosophic-Set. It is an entity of the form $P_{SV}^{a} = \left(< x_i, \mu_{P^a}(x_i), i_{P^a}(x_i), f_{P^a}(x_i) > | x_i \in U\right)$ where $(i)\, \mu_{P^a}(x_i) : U \to [0,1]$ represents a membership-function $(ii)\, i_{P^a}(x_i) : U \to [0,1]$ is an 'indeterminacy-membership-function' and $(iii)\, f_{P^a}(x_i) : U \to [0,1]$ represents a 'falsity-membership-function'. Moreover, each membership function satisfies the essential condition $0 \leq \mu_{P^a}(x_i) + i_{P^a}(x_i) + f_{P^a}(x_i) \leq 3$. Furthermore, the complement $C\left(P_{SV}^{a}\right)$ of $P_{SV}^{a} \subseteq U$ is an object of the form $C\left(P_{SV}^{a}\right) = \left(x_i, f_{P^a}(x_i), 1 - i_{P^a}(x_i), \mu_{P^a}(x_i) | x_i \in U\right)$.

Def. 2.5: Single-Valued Neutrosophic-Entropy. Let $R(U)$ be a well-defined collection of all 'single-valued-neutrosophic-sets' (SVNSs) and $P_{SV}^{a} \in R(U)$. A function $R_N : R(U) \to R^{+}$ is called as a 'single-valued-neutrosophic-entropy' measure if $(i)\, R_N\left(P_{SV}^{a}\right) \geq 0 \forall P_{SV}^{a} \in R(U)$ which vanishes if either $\mu_{P^a}(x_i) = 1, i_{P^a}(x_i) = 0, f_{P^a}(x_i) = 0$ or $\mu_{P^a}(x_i) = 0, i_{P^a}(x_i) = 0, f_{P^a}(x_i) = 1$.

$(ii) R_N\left(P_{SV}^{a}\right)$ satisfies the concavity property with respect to each $\mu_{P^a}(x_i), i_{P^a}(x_i), f_{P^a}(x_i)$. In other words,

$$\frac{\partial^2 R_N\left(P_{FS}^{a}\right)}{\partial \mu_{P^a}^{2}(x_i)} < 0, \frac{\partial^2 R_N\left(P_{FS}^{a}\right)}{\partial i_{P^a}^{2}(x_i)} < 0, \frac{\partial^2 R_N\left(P_{FS}^{a}\right)}{\partial f_{P^a}^{2}(x_i)} < 0 \forall \mu_{P^a}(x_i), i_{P^a}(x_i), f_{P^a}(x_i) \in [0,1].$$

(iii) Because of concavity, $R_N\left(P_{SV}^{a}\right)$ possesses its maximal-value which arises when $\mu_{P^a}(x_i) = i_{P^a}(x_i) = f_{P^a}(x_i) = \frac{1}{2}$. $(iv)\, R_N\left(C\left(P_{SV}^{a}\right)\right) = R_N\left(P_{SV}^{a}\right)$.

Def.2.6: Single-Valued-Neutrosophic-Cross-Entropy : Let $P_{SV}^{a}=\left(<x_i,\mu_{P^a}(x_i),i_{P^a}(x_i),f_{P^a}(x_i)>|\,x_i\in U\right)\&\,Q_{SV}^{a}=\left(<x_i,\mu_{Q^a}(x_i),i_{Q^a}(x_i),f_{Q^a}(x_i)>|\,x_i\in U\right)$ are any two 'single-valued-neutrosophic-sets' in the finite space $U=(x_1,x_2,...,x_n)$ where $(i)\,\mu_{P^a}(x_i),\mu_{Q^a}(x_i):U\to[0,1],(ii)\,i_{P^a}(x_i),i_{Q^a}(x_i):U\to[0,1],(iii)\,f_{P^a}(x_i),f_{Q^a}(x_i):U\to[0,1]$ respectively are true membership, indeterminacy membership and falsity membership degree functions. Then a function $R_{CE}:R(U)\times R(U)\to R^{+}$ is termed as single-valued neutrosophic cross-entropy measure if

$(i)\,R_{CE}\left(P_{SV}^{a},Q_{SV}^{a}\right)\geq 0\forall P_{SV}^{a},Q_{SV}^{a}\in R(U)$ and equality occurs when $P_{SV}^{a}=Q_{SV}^{a}$.

$(ii)\,R_{CE}\left(P_{SV}^{a},Q_{SV}^{a}\right)=R_{CE}\left(Q_{SV}^{a},P_{SV}^{a}\right)$. In other words, $R_{CE}\left(P_{SV}^{a},Q_{SV}^{a}\right)$ is symmetric in nature.

$(iii)\,R_{CE}\left(C\left(P_{SV}^{a}\right),C\left(Q_{SV}^{a}\right)\right)=R_{CE}\left(P_{SV}^{a},Q_{SV}^{a}\right)$ which means $R_{CE}\left(P_{SV}^{a},Q_{SV}^{a}\right)$ does not change whenever $P_{SV}^{a}\,\&\,Q_{SV}^{a}$ are replaced by $C\left(P_{SV}^{a}\right)$ and $C\left(Q_{SV}^{a}\right)$.

2.2 Novel Hyperbolic Fuzzy-Entropy-Measure (HFE) Measure

To meet the required goals, first establish a hyperbolic fuzzy-entropy measure (**Theorem 2.1)** which will be a determination for the development of another novel symmetric fuzzy-cross-entropy measure hinged on two 'fuzzy-sets' (**Theorem 2.2).**

Theorem 2.1. Let $P_{FS}^{a}=\left(<x_i,\mu_{P^a}(x_i)>|\,x_i\in U\right)$ be any fuzzy set in U. Then $H_{FS}\left(P_{FS}^{a}\right)$ is an authentic hyperbolic-fuzzy-entropy measure **(Def.2.2)** defined by

$$H_{FS}\left(P_{FS}^{a}\right)=-\sum_{i=1}^{n}\left[Sinh\left(\frac{1+\mu_{P^a}^{2}(x_i)+\left(1-\mu_{P^a}(x_i)\right)^{2}}{8+\left(\sqrt{\mu_{P^a}(x_i)}+\sqrt{1-\mu_{P^a}(x_i)}\right)^{4}}\right)-Sinh\left(\frac{2}{9}\right)\right]\qquad\ldots(1)$$

which assumes its lowest value of zero and maximum as $\left(Sinh\frac{2}{9}-Sinh\frac{1}{8}\right)n.$ Here, $\mu_{P^a}(x_i)$ denotes the fuzziness of $'i^{th}'$ energy value and $H_{FS}\left(P_{FS}^{a}\right)$ denote the amount of fuzziness indicated by the fuzzy set P_{FS}^{a}.

Proof (i) $H_{FS}\left(P_{FS}^{a}\right)\geq 0\forall P_{FS}^{a}\in F(U)$ with equality if $\mu_{P^a}(x_i)=0$ or $1\forall i=1,2,...,n.$

(ii) $H_{FS}\left(C\left(P_{FS}^{a}\right)\right)=H_{FS}\left(P_{FS}^{a}\right)$. This means $H_{FS}\left(P_{FS}^{a}\right)$ does not change after replacing $\mu_{P^a}\left(x_i\right)$ with $1-\mu_{P^a}\left(x_i\right)$ into **(1).**

(iii) **Concavity:** The hyperbolic fuzzy entropy $H_{FS}\left(P_{FS}^{a}\right)$ can be differentiated partially because the positive term finite series in **(1)** is absolutely and uniformly convergent and hence possesses first and second order partial derivatives. Mathematica software (Wolfram) yields

$$\frac{\partial H_{FS}\left(P_{FS}^{a}\right)}{\partial \mu_{P^a}\left(x_i\right)}$$

$$=\frac{2\left(1-2\mu_{P^a}\left(x_i\right)\right)\left(2+2\mu_{P^a}\left(x_i\right)-2\mu_{P^a}^{2}\left(x_i\right)+13\sqrt{\mu_{P^a}\left(x_i\right)\left(1-\mu_{P^a}\left(x_i\right)\right)}\right)Cosh\left(\frac{2\left(1-\mu_{P^a}\left(x_i\right)+\mu_{P^a}^{2}\left(x_i\right)\right)}{8+\left(\sqrt{\mu_{P^a}\left(x_i\right)}+\sqrt{1-\mu_{P^a}\left(x_i\right)}\right)^{4}}\right)}{\sqrt{\mu_{P^a}\left(x_i\right)\left(1-\mu_{P^a}\left(x_i\right)\right)}\left(9+4\mu_{P^a}\left(x_i\right)-4\mu_{P^a}^{2}\left(x_i\right)+4\sqrt{\mu_{P^a}\left(x_i\right)\left(1-\mu_{P^a}\left(x_i\right)\right)}\right)^{2}}\quad\ldots(2)$$

$$\frac{\partial^2 H_{FS}\left(P_{FS}^{a}\right)}{\partial \mu_{P^a}^{2}\left(x_i\right)}$$

$$=-\left[\begin{array}{l}\dfrac{2\left(9+4\mu_{P^a}\left(x_i\right)-4\mu_{P^a}^{2}\left(x_i\right)+4\sqrt{\mu_{P^a}\left(x_i\right)\left(1-\mu_{P^a}\left(x_i\right)\right)}\right)}{3\sqrt{\mu_{P^a}\left(x_i\right)\left(1-\mu_{P^a}\left(x_i\right)\right)}}\times \\ \left\{Cosh\left(\dfrac{2\left(1-\mu_{P^a}\left(x_i\right)+\mu_{P^a}^{2}\left(x_i\right)\right)}{8+\left(\sqrt{\mu_{P^a}\left(x_i\right)}+\sqrt{1-\mu_{P^a}\left(x_i\right)}\right)^{4}}\right)\left(\begin{array}{l}9+63\mu_{P^a}\left(x_i\right)-147\mu_{P^a}^{2}\left(x_i\right)+136\mu_{P^a}^{3}\left(x_i\right)+12\mu_{P^a}^{4}\left(x_i\right) \\ +310\sqrt{\left(1-\mu_{P^a}\left(x_i\right)\right)}\mu_{P^a}^{\frac{3}{2}}\left(x_i\right)-622\sqrt{\left(1-\mu_{P^a}\left(x_i\right)\right)}\mu_{P^a}^{\frac{5}{2}}\left(x_i\right) \\ +624\sqrt{\left(1-\mu_{P^a}\left(x_i\right)\right)}\mu_{P^a}^{\frac{7}{2}}\left(x_i\right)-312\sqrt{\left(1-\mu_{P^a}\left(x_i\right)\right)}\mu_{P^a}^{\frac{9}{2}}\left(x_i\right) \\ -96\mu_{P^a}^{5}\left(x_i\right)+32\mu_{P^a}^{6}\left(x_i\right)+12\sqrt{\mu_{P^a}\left(x_i\right)\left(1-\mu_{P^a}\left(x_i\right)\right)}\end{array}\right)\right\} \\ \dfrac{-\dfrac{4\left(1-24\mu_{P^a}\left(x_i\right)\right)^{2}}{\mu_{P^a}\left(x_i\right)\left(1-\mu_{P^a}\left(x_i\right)\right)}\left\{\left(\begin{array}{l}2+2\mu_{P^a}\left(x_i\right)-2\mu_{P^a}^{2}\left(x_i\right) \\ +13\sqrt{\mu_{P^a}\left(x_i\right)\left(1-\mu_{P^a}\left(x_i\right)\right)}\end{array}\right)Sinh\left(\dfrac{2\left(1-\mu_{P^a}\left(x_i\right)+\mu_{P^a}^{2}\left(x_i\right)\right)}{8+\left(\sqrt{\mu_{P^a}\left(x_i\right)}+\sqrt{1-\mu_{P^a}\left(x_i\right)}\right)^{4}}\right)\right\}}{\left(9+4\mu_{P^a}\left(x_i\right)-4\mu_{P^a}^{2}\left(x_i\right)+4\sqrt{\mu_{P^a}\left(x_i\right)\left(1-\mu_{P^a}\left(x_i\right)\right)}\right)^{3}}\end{array}\right]\leq 0$$

for each $\mu_{P^a}\left(x_i\right)\in[0,1]$ which authenticates the concavity of $H_{FS}\left(P_{FS}^{a}\right)$ with respect to each $\mu_{P^a}\left(x_i\right)$. The fact that $H_{FS}\left(P_{FS}^{a}\right)$ is a concave function of $\mu_{P^a}\left(x_i\right)$ can also be experienced from its 3-dimensional rotational plot **(Fig.2).**

(iv)Due to concavity property of $H_{FS}\left(P_{FS}^{a}\right)$ with respect to $\mu_{P^a}\left(x_i\right)$, there exists a maximum value which arises when $\frac{\partial\, H_{FS}\left(P_{FS}^{a}\right)}{\partial \mu_{P^a}\left(x_i\right)}=0.$ In view of equation **(1),** this yields

$\tilde{\mu}_{A^w}(x_i)=\frac{1}{2}.$ Also, Max. $H_{FS}\left(P_{FS}^{a}\right)=\left(Sinh\frac{2}{9}-Sinh\frac{1}{8}\right)n$ … (3)

Theorem 2.2 Let $P_{FS}^{a}=\left(<x_i,\mu_{P^a}\left(x_i\right)>|\, x_i\in U\right)$ and $Q_{FS}^{a}=\left(<x_i,\mu_{Q^a}\left(x_i\right)>|\, x_i\in U\right)$ are any two fuzzy sets in $U=\left(x_1,x_2,...,x_n\right)$. Show that $H_{CE}^{\mu}\left(P_{FS}^{a},Q_{FS}^{a}\right)$ is a valid symmetric-hyperbolic fuzzy-cross-entropy or discrimination information measure **(Def. 2.3)** hinged on two 'fuzzy-sets' P_{FS}^{a} and Q_{FS}^{a} taken

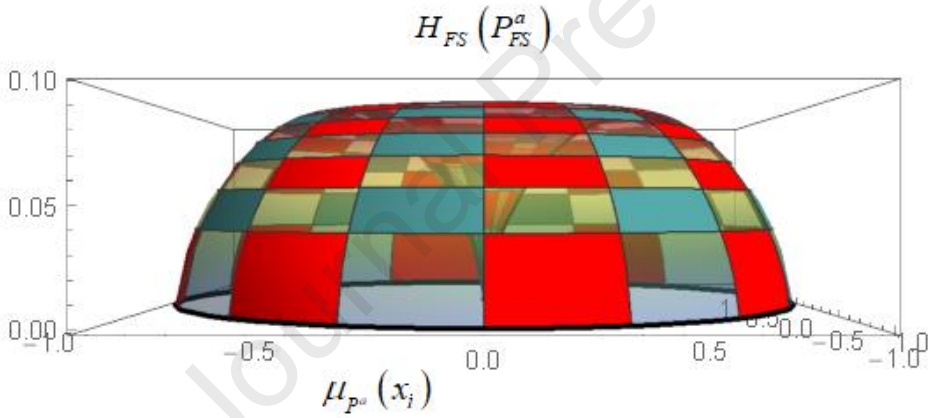

Fig.2. Concavity of $H_{FS}\left(P_{FS}^{a}\right)$ with respect to $\mu_{P^a}\left(x_i\right)$.

$$H_{CE}^{\mu}\left(P_{FS}^{a},Q_{FS}^{a}\right)=\sum_{i=1}^{n}\left[-6Sinh\left(\frac{1}{8}\right)+\left(2+\mu_{P^a}\left(x_i\right)+\mu_{Q^a}\left(x_i\right)\right)Sinh\left(\frac{1+\mu_{P^a}^{2}\left(x_i\right)+\mu_{Q^a}^{2}\left(x_i\right)}{8+\left(\sqrt{\mu_{P^a}\left(x_i\right)}+\sqrt{\mu_{Q^a}\left(x_i\right)}\right)^{4}}\right)+\left(4-\mu_{P^a}\left(x_i\right)-\mu_{Q^a}\left(x_i\right)\right)Sinh\left(\frac{1+\left(1-\mu_{P^a}\left(x_i\right)\right)^{2}+\left(1-\mu_{Q^a}\left(x_i\right)\right)^{2}}{8+\left(\sqrt{1-\mu_{P^a}\left(x_i\right)}+\sqrt{1-\mu_{Q^a}\left(x_i\right)}\right)^{4}}\right)\right]$$ … (4)

It is informative to note that $H_{CE}^{\mu}\left(P_{FS}^{a},Q_{FS}^{a}\right)$ represents the mathematical-value of true membership degree based on the 'symmetric-discrimination' of P_{FS}^{a} against Q_{FS}^{a}.

Proof. In view of **Def.2.3,** $H_{CE}^{\mu}\left(C\left(P_{FS}^{a}\right),C\left(Q_{FS}^{a}\right)\right)=H_{CE}^{\mu}\left(P_{FS}^{a},Q_{FS}^{a}\right)$ is straightforward for each $P_{FS}^{a},Q_{FS}^{a}\in F\left(U\right)$. Also, the symmetry property in view of **Def.2.3** is true

because $H_{CE}^{\mu}\left(P_{FS}^{a},Q_{FS}^{a}\right)=H_{CE}^{\mu}\left(Q_{FS}^{a},P_{FS}^{a}\right)$. To get the non-negativity of $H_{CE}^{\mu}\left(P_{FS}^{a},Q_{FS}^{a}\right)$, first divert to establish the given **Lemma 2.1.**

Lemma 2.1 If $P_1\left(\mu_{P^a}(x_i),\mu_{Q^a}(x_i)\right)=\sqrt{\frac{\mu_{p^a}^2(x_i)+\mu_{Q^a}^2(x_i)}{2}}$ and $P_2=\left(\frac{\sqrt{\mu_{P^a}(x_i)}+\sqrt{\mu_{Q^a}(x_i)}}{2}\right)^2$,

Then there exist the inequality $P_1\geq P_2$ with equality if $\mu_{P^a}(x_i)=\mu_{Q^a}(x_i)\forall i=1,2,...,n.$

Proof: The bias can be taken true if $P_1\geq P_2$ or if

$$\sqrt{\frac{\mu_{p^a}^2(x_i)+\mu_{Q^a}^2(x_i)}{2}}\geq\left(\frac{\mu_{P^a}(x_i)+\mu_{Q^a}(x_i)+2\sqrt{\mu_{P^a}(x_i)\mu_{Q^a}(x_i)}}{4}\right) \text{ or if}$$

$$8\left(\mu_{p^a}^2(x_i)+\mu_{Q^a}^2(x_i)\right)\geq\mu_{p^a}^2(x_i)+\mu_{Q^a}^2(x_i)+6\mu_{P^a}(x_i)\mu_{Q^a}(x_i)+4\sqrt{\mu_{P^a}(x_i)}\sqrt{\mu_{Q^a}(x_i)}\left(\mu_{P^a}(x_i)+\mu_{Q^a}(x_i)\right)$$

$$\Rightarrow 7\mu_{p^a}^2(x_i)+7\mu_{Q^a}^2(x_i)-6\mu_{P^a}(x_i)\mu_{Q^a}(x_i)-4\sqrt{\mu_{P^a}(x_i)}\sqrt{\mu_{Q^a}(x_i)}\left(\mu_{P^a}(x_i)+\mu_{Q^a}(x_i)\right)\geq 0$$

which is obviously true for each $\mu_{P^a}(x_i),\mu_{Q^a}(x_i)\in[0,1]$. Also, the equality occurs, that is,

$P_1=P_2$ if $\mu_{P^a}(x_i)=\mu_{Q^a}(x_i)\forall i=1,2,...,n.$

Thus, with the aid of resulting **Lemma- 2.1,** the $P_1\geq P_2$ bias can be re-designed

$$\frac{\mu_{p^a}^2(x_i)+\mu_{Q^a}^2(x_i)}{2}\geq\left(\frac{\sqrt{\mu_{P^a}(x_i)}+\sqrt{\mu_{Q^a}(x_i)}}{2}\right)^4$$

$$\Rightarrow \mu_{p^a}^2(x_i)+\mu_{Q^a}^2(x_i)+1\geq\frac{\left(\sqrt{\mu_{P^a}(x_i)}+\sqrt{\mu_{Q^a}(x_i)}\right)^4}{8}+1$$

$$\Rightarrow \frac{\mu_{p^a}^2(x_i)+\mu_{Q^a}^2(x_i)+1}{8+\left(\sqrt{\mu_{P^a}(x_i)}+\sqrt{\mu_{Q^a}(x_i)}\right)^4}\geq\frac{1}{8} \qquad \text{..... (5)}$$

Using the monotonicity of sine-hyperbolic function over $[0,1]$, the inequality **(5)** yields

$$\left(2+\mu_{P^a}(x_i)+\mu_{Q^a}(x_i)\right)Sinh\left(\frac{1+\mu_{p^a}^2(x_i)+\mu_{Q^a}^2(x_i)}{8+\left(\sqrt{\mu_{P^a}(x_i)}+\sqrt{\mu_{Q^a}(x_i)}\right)^4}\right)\geq\left(2+\mu_{P^a}(x_i)+\mu_{Q^a}(x_i)\right)Sinh\left(\frac{1}{8}\right)...(6)$$

Replacement of $\mu_{P^a}(x_i),\mu_{Q^a}(x_i)$ with their counterparts $1-\mu_{P^a}(x_i),1-\mu_{Q^a}(x_i)$ into the resulting inequality **(5)** yields

$$\left(4-\mu_{P^a}(x_i)-\mu_{Q^a}(x_i)\right)Sinh\left(\frac{1+\left(1-\mu_{P^a}(x_i)\right)^2+\left(1-\mu_{Q^a}(x_i)\right)^2}{8+\left(\sqrt{1-\mu_{P^a}(x_i)}+\sqrt{1-\mu_{Q^a}(x_i)}\right)^4}\right)\geq\left(4-\mu_{P^a}(x_i)-\mu_{Q^a}(x_i)\right)Sinh\left(\frac{1}{8}\right)\ldots(7)$$

The desired result , that is, $H_{CE}^{\mu}\left(P_{FS}^a,Q_{FS}^a\right)\geq 0\forall\mu_{P^a}(x_i),\mu_{Q^a}(x_i)\in[0,1]$ can be easily obtained after adding the bias **(5, 6)** and taking the sum over $i=1$ to $i=n$. Also, $H_{CE}^{\mu}\left(P_{FS}^a,Q_{FS}^a\right)$ vanishes if $\mu_{P^a}(x_i)=\mu_{Q^a}(x_i)\forall i=1,2,...,n.$

Our next **Theorem 2.3** will discuss the situation under which $H_{CE}^{\mu}\left(P_{FS}^a,Q_{FS}^a\right)$ admits its maximum and minimum value.

Theorem 2.3 Let $P_{FS}^a=\left(<x_i,\mu_{P^a}(x_i)>|\,x_i\in U\right)$ and $Q_{FS}^a=\left(<x_i,\mu_{Q^a}(x_i)>|\,x_i\in U\right)$ are any 02 'fuzzy-sets' with equal cardinality in $U=(x_1,x_2,...,x_n)$. Then there is a issue of inequity: $0\leq H_{CE}^{\mu}\left(P_{FS}^a,Q_{FS}^a\right)\leq 6\left(Sinh\frac{2}{9}-Sinh\frac{1}{8}\right)n.$

Proof. The final expression **(4)** with the replacement of Q_{FS}^a with $C\left(P_{FS}^a\right)$

$$H_{CE}^{\mu}\left(P_{FS}^a,C\left(P_{FS}^a\right)\right)=\sum_{i=1}^{n}\left[-6Sinh\left(\frac{1}{8}\right)+6Sinh\left(\frac{1+\mu_{p^a}^2(x_i)+\left(1-\mu_{P^a}(x_i)\right)^2}{8+\left(\sqrt{\mu_{P^a}(x_i)}+\sqrt{1-\mu_{P^a}(x_i)}\right)^4}\right)\right] \quad \ldots (8)$$

$$=\sum_{i=1}^{n}\left[6\left(Sinh\frac{2}{9}-Sinh\frac{1}{8}\right)-6\left(Sinh\frac{2}{9}-Sinh\left(\frac{1+\mu_{p^a}^2(x_i)+\left(1-\mu_{P^a}(x_i)\right)^2}{8+\left(\sqrt{\mu_{P^a}(x_i)}+\sqrt{1-\mu_{P^a}(x_i)}\right)^4}\right)\right)\right] \quad \ldots (9)$$

$$=6\,Max.H_{FS}\left(P_{FS}^a\right)-6H_{FS}\left(P_{FS}^a\right) \quad \ldots (10)$$

From **Theorem 2.1,** $H_{FS}\left(P_{FS}^a\right)\geq 0\forall P_{FS}^a\in F(U)$ and hence **(10)** yields

$$0\leq H_{CE}^{\mu}\left(P_{FS}^a,C\left(P_{FS}^a\right)\right)\leq 6\left(Sinh\frac{2}{9}-Sinh\frac{1}{8}\right)n \quad \ldots (11)$$

Since n is finite, the resulting inequality **(11)** justifies that $H_{CE}^{\mu}\left(P_{FS}^a,C\left(P_{FS}^a\right)\right)$ is bounded by two finite quantities. Following the same pattern, one can easily show that $H_{CE}^{\mu}\left(P_{FS}^a,Q_{FS}^a\right)$ is also bounded between two finite quantities, which are respectively minimum and maximum

values of $H_{CE}^{\mu}\left(P_{FS}^{a},Q_{FS}^{a}\right)$This maximum value is independent of the entities of U, but completely depends on its cardinality **[25-27]**. The fact that $H_{CE}^{\mu}\left(P_{FS}^{a},Q_{FS}^{a}\right)$ confirms its least possible value 'zero' can be seen from 3D plot ; **Fig. 3(a).** In addition to this, the 3-dimensional region plot **Fig.3(b)** confirms that $H_{CE}^{\mu}\left(P_{FS}^{a},Q_{FS}^{a}\right)$increases with the increase in the amount of $\left|P_{FS}^{a}-Q_{FS}^{a}\right|$, achieves its maximum value $6\left(Sinh\frac{2}{9}-Sinh\frac{1}{8}\right)n$ at the points $(1,0)$ & $(0,1)$ and minimum value zero at $(0,0)$.

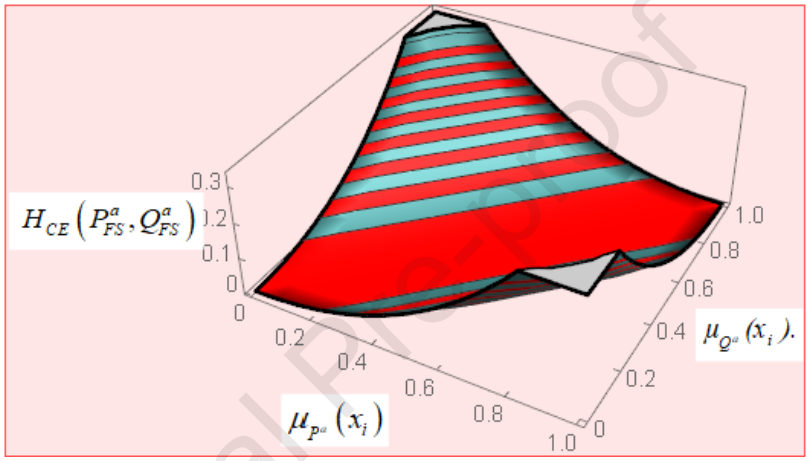

(a)

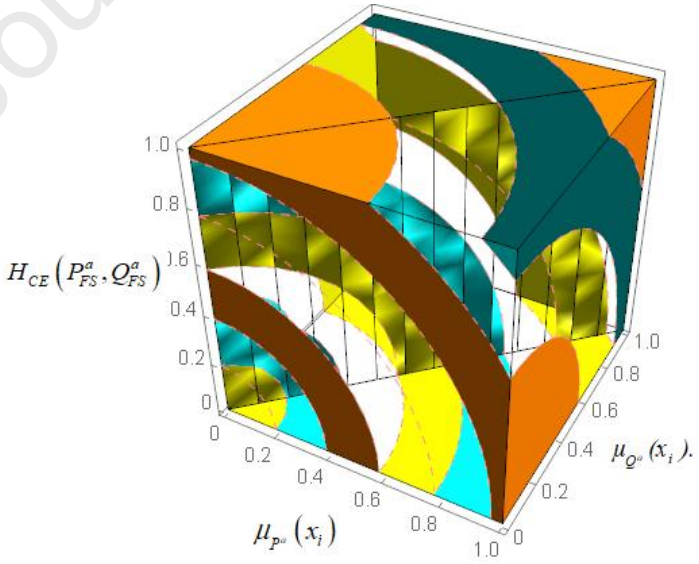

(b)

Fig.3. Hyperbolic Fuzzy Cross Entropy-Measure Maximum and Minimum Values $H_{CE}^{\mu}\left(P_{FS}^{a},Q_{FS}^{a}\right)$

The aftermaths of resulting **Theorems 2.1-2.3** will be deployed to get proclaimed 'single valued-neutrosophic-entropy-measure', the result of which will play an eminent-role in optimizing the FSP parameters.

2.3 Hyperbolic Single -Valued-Neutrosophic-Entropy (NFE)

It is a solid-position to extend the symmetric hyperbolic fuzzy-cross-entropy measure based on two-fuzzy-sets to this part based on two 'single-valued neutrosophic-sets'.

Def. 2.7 Suppose there are two 'single-valued the neutrosophic-sets' **(Def.2.4)** represented by

$P_{SV}^{a} = \left(< x_i, \mu_{P^a}(x_i), i_{P^a}(x_i), f_{P^a}(x_i) > | \, x_i \in U \right)$ and $Q_{SV}^{a} = \left(< x_i, \mu_{Q^a}(x_i), i_{Q^a}(x_i), f_{Q^a}(x_i) > | \, x_i \in U \right)$

In view of resulting **Theorems 2,** the proffered symmetric fuzzy cross-entropy measure $H_{CE}^{\mu}\left(P_{FS}^{a}, Q_{FS}^{a}\right)$ represents the mathematical-value of 'true-membership-degree' based on a 'symmetric-discrimination' of P_{FS}^{a} against Q_{FS}^{a}. If $H_{CE}^{i}\left(P_{FS}^{a}, Q_{FS}^{a}\right)$ and $H_{CE}^{f}\left(P_{FS}^{a}, Q_{FS}^{a}\right)$ respectively denote the mathematical values of indeterminacy and falsity membership degrees based on symmetric discriminations of P_{FS}^{a} against Q_{FS}^{a}, then

$$H_{CE}^{i}\left(P_{FS}^{a}, Q_{FS}^{a}\right) = \sum_{i=1}^{n}\left[-6Sinh\left(\frac{1}{8}\right) + \left(2 + i_{P^a}(x_i) + i_{Q^a}(x_i)\right) Sinh\left(\frac{1 + i_{P^a}^{2}(x_i) + i_{Q^a}^{2}(x_i)}{8 + \left(\sqrt{i_{P^a}(x_i)} + \sqrt{i_{Q^a}(x_i)}\right)^{4}} \right) + \left(4 - i_{P^a}(x_i) - i_{Q^a}(x_i)\right) Sinh\left(\frac{1 + \left(1 - i_{P^a}(x_i)\right)^{2} + \left(1 - i_{Q^a}(x_i)\right)^{2}}{8 + \left(\sqrt{1 - i_{P^a}(x_i)} + \sqrt{1 - i_{Q^a}(x_i)}\right)^{4}} \right) \right] \quad \ldots (12)$$

$$H_{CE}^{f}\left(P_{FS}^{a}, Q_{FS}^{a}\right) = \sum_{i=1}^{n}\left[-6Sinh\left(\frac{1}{8}\right) + \left(2 + f_{P^a}(x_i) + f_{Q^a}(x_i)\right) Sinh\left(\frac{1 + f_{P^a}^{2}(x_i) + f_{Q^a}^{2}(x_i)}{8 + \left(\sqrt{f_{P^a}(x_i)} + \sqrt{f_{Q^a}(x_i)}\right)^{4}} \right) + \left(4 - f_{P^a}(x_i) - f_{Q^a}(x_i)\right) Sinh\left(\frac{1 + \left(1 - f_{P^a}(x_i)\right)^{2} + \left(1 - f_{Q^a}(x_i)\right)^{2}}{8 + \left(\sqrt{1 - f_{P^a}(x_i)} + \sqrt{1 - f_{Q^a}(x_i)}\right)^{4}} \right) \right] \quad \ldots (13)$$

Simply addition of resulting expressions **(4), (12)** and **(13)** will yield the desired symmetric hyperbolic' single-valued-neutrosophic cross-entropy-measure', denoted by $R_{CE}\left(P_{SV}^{a}, Q_{SV}^{a}\right)$, hinged on two SVNSs P_{FS}^{a} and Q_{FS}^{a} as follows.

$$R_{CE}\left(P_{SV}^{a}, Q_{SV}^{a}\right) = H_{CE}^{\mu}\left(P_{FS}^{a}, Q_{FS}^{a}\right) + H_{CE}^{i}\left(P_{FS}^{a}, Q_{FS}^{a}\right) + H_{CE}^{f}\left(P_{FS}^{a}, Q_{FS}^{a}\right) \quad \ldots (14)$$

The resulting expression **(14)** satisfies all the essential conditions notified in **Def.2.6** and indicates the mathematical value based on true, 'indeterminacy and falsity membership degrees' of symmetric discriminations of P_{SV}^{a} against Q_{SV}^{a}.

Theorem 2.4 Let

$P_{SV}^{a}=\left(<x_i,\mu_{P^a}(x_i),i_{P^a}(x_i),f_{P^a}(x_i)>|\,x_i\in U\right)$ and $Q_{SV}^{a}=\left(<x_i,\mu_{Q^a}(x_i),i_{Q^a}(x_i),f_{Q^a}(x_i)>|\,x_i\in U\right)$ be two singles valued as of $U=(x_1,x_2,...,x_n)$. Then, there exists the diversity:

$$0\le R_{CE}\left(P_{SV}^{a},Q_{SV}^{a}\right)\le 18\left(Sinh\frac{2}{9}-Sinh\frac{1}{8}\right)n.$$

Proof. To replace Q_{SV}^{a} with $C\left(Q_{SV}^{a}\right)$ into the resulting-expression **(14)** gets

$$R_N\left(P_{SV}^{a},C\left(P_{SV}^{a}\right)\right)=\sum_{i=1}^{n}\left[18Sinh\left(\frac{2}{9}\right)-18Sinh\left(\frac{1}{8}\right)-6\left(\begin{array}{l}3Sinh\left(\frac{2}{9}\right)-\left(\frac{2+\mu_{P^a}(x_i)+f_{P^a}(x_i)}{3}\right)Sinh\left(\frac{1+\mu_{p^a}^{2}(x_i)+f_{Q^a}^{2}(x_i)}{8+\left(\sqrt{\mu_{P^a}(x_i)}+\sqrt{f_{P^a}(x_i)}\right)^{4}}\right)\\-\left(\frac{4-\mu_{P^a}(x_i)-f_{P^a}(x_i)}{3}\right)Sinh\left(\frac{1+\left(1-\mu_{P^a}(x_i)\right)^{2}+\left(1-f_{P^a}(x_i)\right)^{2}}{8+\left(\sqrt{1-\mu_{P^a}(x_i)}+\sqrt{1-f_{P^a}(x_i)}\right)^{4}}\right)\\-Sinh\left(\frac{1+i_{p^a}^{2}(x_i)+\left(1-i_{P^a}(x_i)\right)^{2}}{8+\left(\sqrt{i_{P^a}(x_i)}+\sqrt{1-i_{P^a}(x_i)}\right)^{4}}\right)\end{array}\right)\right]$$

$$=6\,\mathrm{Max}.R_N\left(P_{SV}^{a}\right)-R_N\left(P_{SV}^{a}\right);\qquad\ldots(15)$$

$$R_N\left(P_{SV}^{a}\right)=\sum_{i=1}^{n}\left[\begin{array}{l}3Sinh\left(\frac{2}{9}\right)-Sinh\left(\frac{1+i_{p^a}^{2}(x_i)+\left(1-i_{P^a}(x_i)\right)^{2}}{8+\left(\sqrt{i_{P^a}(x_i)}+\sqrt{1-i_{P^a}(x_i)}\right)^{4}}\right)-\left(\frac{2+\mu_{P^a}(x_i)+f_{P^a}(x_i)}{3}\right)Sinh\left(\frac{1+\mu_{p^a}^{2}(x_i)+f_{Q^a}^{2}(x_i)}{8+\left(\sqrt{\mu_{P^a}(x_i)}+\sqrt{f_{P^a}(x_i)}\right)^{4}}\right)\\-\left(\frac{4-\mu_{P^a}(x_i)-f_{P^a}(x_i)}{3}\right)Sinh\left(\frac{1+\left(1-\mu_{P^a}(x_i)\right)^{2}+\left(1-f_{P^a}(x_i)\right)^{2}}{8+\left(\sqrt{1-\mu_{P^a}(x_i)}+\sqrt{1-f_{P^a}(x_i)}\right)^{4}}\right)\end{array}\right]\ldots(16)$$

The resulting announcement **(16)** is the required proclaimed hyperbolic 'single-valued neutrosophic-entropy' (HNE) measurement because it appeases all necessary conditions (**Def.2.5)** as follows.

$(i)\,R_N\left(P_{SV}^{a}\right)\ge 0\forall P_{SV}^{a}\in R(U)$ with equality if either $\mu_{P^a}(x_i)=1,i_{P^a}(x_i)=0,f_{P^a}(x_i)=0$ or $\mu_{P^a}(x_i)=0,i_{P^a}(x_i)=0,f_{P^a}(x_i)=1$ $(ii)\,R_N\left(C\left(P_{SV}^{a}\right)\right)=R_N\left(P_{SV}^{a}\right)$ $(iii)R_N\left(P_{SV}^{a}\right)$ is a concave function of $\mu_{P^a}(x_i),i_{P^a}(x_i),f_{P^a}(x_i)$ $(iv)\ 0\le R_{CE}\left(P_{SV}^{a}\right)\le 3\left(Sinh\frac{2}{9}-Sinh\frac{1}{8}\right)n$. The fact $R_N\left(P_{SV}^{a}\right)$ takes the minimum-value as zero can be experienced in the 3D plot **(Fig.4).** Also, **(15)** yields

$$R_N\left(P_{SV}^a\right)=\text{Max}.R_N\left(P_{SV}^a\right)-\frac{1}{6}R_N\left(P_{SV}^a,C\left(P_{SV}^a\right)\right)\geq 0 \quad \ldots (17)$$

$$\Rightarrow 0\leq R_N\left(P_{SV}^a,C\left(P_{SV}^a\right)\right)\leq 18\left(Sinh\left(\frac{2}{9}\right)-Sinh\left(\frac{1}{8}\right)\right)n \quad \ldots (18)$$

Following the similar pattern employed in the resulting **Theorem 2.3,** it is quite easy to establish $0\leq R_{CE}\left(P_{SV}^a,Q_{SV}^a\right)\leq 18\left(Sinh\frac{2}{9}-Sinh\frac{1}{8}\right)n$ where n is the cardinality of U. Thus,

$\text{Max}.R_{CE}\left(P_{SV}^a,Q_{SV}^a\right)=18\left(Sinh\frac{2}{9}-Sinh\frac{1}{8}\right)n$ and $\text{Min}.R_{CE}\left(P_{SV}^a,Q_{SV}^a\right)=0.$

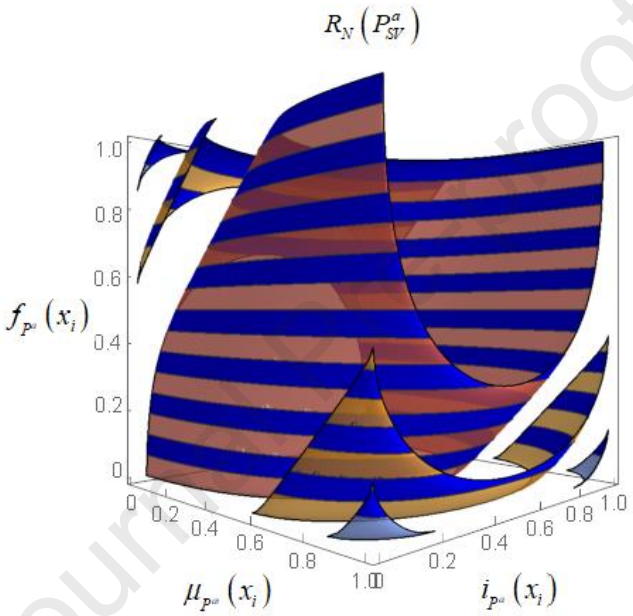

Fig.4. Least value of Hyperbolic Single-valued Neutrosophic-Entropy (HNE).

To authenticate the applicability and effectiveness of the proffered hyperbolic fuzzy entropy **(1)** and single-valued-neutrosophic-entropy **(16)**, we shall equally well deploy these entropy measures for the classification of friction stir process parameters under variable reinforcement conditions as follows from section 2.5 onwards.

2.4. Materials and Methods:

In this study, we have fabricated AA7075 alloy by incorporating B_4C particles. The studies were carried out on a Vertimach V-350 VMC machine manufactured by TAL (Figure 5(a)). (a). The experiments were conducted on this alloy with a sheet thickness of 5 mm with dimensions 180×160×5. The feed rate was modified from 30 to 50 mm/min and the rotating speed was varied from 1600 to 1400 rpm. On AA7075 aluminium alloy, processing was done

with and without the addition of B_4C particles. The studies were performed at a tilt angle namely 3.14˚. To avoid outpouring of B_4C particles, the 'groove' is first 'capped' with an FSP-like tool without a pin, as shown in Fig.5(b). Furthermore, studies were done on tapered-tool made up of H-13 material with some suitable dimensions. Fig.5(c) shows the tapered tool used for processing.

(a)

(b)

(c)

Fig.5. (a) TAL V-350 CNC Machine; (b) Tool for capping; (c) Tools for processing.

2.5. Entropy Based Methodology for Classifying FST parameters

Step:-1 This experimental research work overviews the analysis of vibrations signal which was carried out by using Data Acquisition System (DAQ) and further analyzed in MATLAB software. The Fast-Fourier Transform of the vibration-signal was generated for analyzing the dispersion and peaks in the signal.

Step:-2 Normalization of Monitored Energy Reading of Processing Parameters

Suppose there are "n" friction stir processed parameters under study and "m"be the number of sub-frequency bands. Let v_{ji} denotes the monitored energy reading of the j^{th} processing parameter at i^{th} sub-frequency band. It is mandatory to normalize all monitored energy readings which can be done by constructing the normalization construction function V_{ji} as follows

$$V_{ji} = \frac{v_{ji} - \text{Min}.v_{ji}}{\text{Max}.v_{ji} - \text{Min}.v_{ji}}; j = 1,2,...n, i = 1,2,...,m.$$

Step:-3 Establishment of Energy Interval Ranges

Suppose the knowledge of familiar faults acquainted by some rotor element in this study is expressed as A_K. Let $\tilde{\mu}_{P_K}(x_i)$ and $\tilde{U}_{P_K}(x_i)$ denote the least and last 'energy-bounds' extracted from the normalization construction function of K^{th} processing parameter at i^{th} sub-frequency-band(s), Then

$$A_K = \left(< x_1, \left[\tilde{\mu}_{A_K}(x_1), \tilde{U}_{A_K}(x_1)\right] >, < x_2, \left[\tilde{\mu}_{A_K}(x_2), \tilde{U}_{A_K}(x_2)\right] >, ..., < x_m, \left[\tilde{\mu}_{A_K}(x_m), \tilde{U}_{A_K}(x_m)\right] >\right)$$

It is informative to underline that $\tilde{\mu}_{A_K}(x_i)$ represents the amount of fuzziness, indicated by the normalization construction function of K^{th} processing parameter at i^{th} 'sub-frequency-band(s)'.

Step:-4: Extension of Energy Interval Ranges into the Form of Fuzzy and Single-Valued Neutrosophic-Sets

The acquitted vibration data, in general, is conflicting and hence should be converted to the form's fuzzy sets as well as 'single-valued-neutrosophic-sets' in order to experience macroscopic optimization of friction stir processed parameters. This conversion, however not problematic, but circumspect and can be done as follows.

Let $\tilde{f}_{A_K}(x_i) = 1 - \tilde{U}_{A_K}(x_i)$ and $\tilde{i}_{A_K}(x_i) = 1 - \tilde{f}_{A_K}(x_i) - \tilde{U}_{A_K}(x_i)$ indicates the amount of fuzziness (normalized-energy) predicated on falsity and 'indeterminancy-membership-grade' or degree

of K^{th} friction stir processed parameter at i^{th} sub-frequency band consecutively. In this study, we have restricted all those values of $i^{*}_{A_K}(x_i)$ to zero which are less than zero. Under these conditions, the set A_K can be extended into the desired forms as follows:

(a) Into the forms of 'fuzzy-sets'. The expanded-version of A_K forms

$$A_K = \left(\left(< x_1, \tilde{\mu}_{A_K}(x_1) > \right), \left(< x_2, \tilde{\mu}_{A_K}(x_2) > \right), ..., \left(x_m, \tilde{\mu}_{A_K}(x_m) \right) \right)$$

(b) Into the forms of neutrosophic sets with a single value. The desired conversion of P_K into this form can be obtained as

$$A_K = \left(\left(< x_1, \tilde{\mu}_{A_K}(x_1), \tilde{i}_{A_K}(x_1), \tilde{f}_{A_K}(x_1) > \right), \left(< x_2, \tilde{\mu}_{A_K}(x_2), \tilde{i}_{A_K}(x_2), \tilde{f}_{A_K}(x_2) > \right), ..., \left(< x_m, \tilde{\mu}_{A_K}(x_m), \tilde{i}_{A_K}(x_m), \tilde{f}_{A_K}(x_m) > \right) \right)$$

Step: -5 Computing HFE and HNE Values of Each A_K

The hyperbolic fuzzy-entropy values $H_{FS}(A_K)$ as well as 'single-valued-neutrosophic-entropy' values $R_N(A_K)$ can be evaluated employing the resulting equations **(1)** and **(16)** consecutively.

Step:-6 Identifying the Most Superlative Processing Parameter

The maximum hyperbolic fuzzy entropy (HFE) value $H_{FS}(A_K)$ or 'single-valued-neutrosophic-entropy' (HNE) value $R_N(A_K)(K = 1,2,...,n)$ is assigned to the most dominant processing parameter.

2.6. Application of Entropy Based Methodology

The proposed approach described in Section 6 is used to begin the process of classifying friction stir processing parameters. The processing parameters number is nine $(n = 9)$ and the number sub-frequency bands is one $(m = 1)$. In order to do so, we represent the various processing parameters by the set $A_K(K = 1,2,3,...,9)$ defined by A_1 = 1400-30, A_2 = 1500-30, A_3 = 1600-30, A_4 = 1400-40, A_5 = 1500-40, A_6 = 1600-40, A_7 = 1400-50, A_8 = 1500-50, A_9 = 1600-50 where the former numeric in A_K represents tool rotational-speed and later represent the feed-rate.The process involved in decomposing the vibration signals through Fast Fourier transforms is already explained in Step 1and the procedure of how to construct normalization construction function is provided in Step 2 of Section 6. We next proceed as follows.

Step:-3 After data comparison, it becomes able to extract the minimum and maximum normalized energy bound of all the nine processing parameters and the results are displayed in **Table 2.** In this study, we have computed the energy interval ranges, denoted by $\left[\bar{\mu}_{P_K}(x_i), \bar{U}_{P_K}(x_i)\right]$, for each $A_K\left(K=1,2,3,...,9\right)$ and the results are displayed in **Table 2 and 3.** However, in view of resulting **Theorem 2.1,** the extracted lower bound $\bar{\mu}_{P_K}(x_i)$ does not satisfy the mandatory condition $0 \le \bar{\mu}_{P_K}(x_i) \le 1$. To meet this exigency, we have squared each $\bar{\mu}_{P_K}(x_i)$, by keeping in mind the fact that if a real number is minimum, so its square would be, and obtained the modified energy interval ranges $\left[\tilde{\mu}_{P_K}(x_i), \tilde{U}_{P_K}(x_i)\right]$ for each $A_K\left(K=1,2,3,...,9\right)$ as shown in **Table 2 and 3.**

Step:-4 The modified energy interval-ranges are extended further to the forms of neutrosophic-sets (single- valued) by replacing $\mu_{P^a}(x_i), i_{P^a}(x_i), f_{P^a}(x_i)$ with $\tilde{\mu}_{A_K}(x_i), \tilde{i}_{A_K}(x_i), \tilde{f}_{A_K}(x_i)$ and the results are given in **Table 2 and 3.**

Step:-5 The entropy measure $H_{FS}(A_K)$ can be re-designed by replacing $\mu_{P^a}(x_i)$ with $\tilde{\mu}_{A_K}(x_i)$ into **(1)** which yields

$$H_{FS}(A_K) = -\sum_{i=1}^{m}\left[Sinh\left(\frac{1+\tilde{\mu}^2_{A_K}(x_i)+\left(1-\tilde{\mu}_{A_K}(x_i)\right)^2}{8+\left(\sqrt{\tilde{\mu}_{A_K}(x_i)}+\sqrt{1-\tilde{\mu}_{A_K}(x_i)}\right)^4}\right)-Sinh\left(\frac{2}{9}\right)\right]; 0 \le \tilde{\mu}_{A_K}(x_i) \le 1 \forall i = 1,2,...,m$$

The various hyperbolic fuzzy entropy values $H_{FS}(A_K)\left(K=1,2,...,9\right)$ are computed employing **(1)** and the results are displayed in **Table 2 and 3.**

Similarly, the neutrosophic entropy measure $R_N(A_K)$ can be re-designed by replacing $\mu_{P^a}(x_i), i_{P^a}(x_i), f_{P^a}(x_i)$ with $\tilde{\mu}_{A_K}(x_i), \tilde{i}_{A_K}(x_i), \tilde{f}_{A_K}(x_i)$ into **(16)** which yields

$$R_N(A_k) = \sum_{i=1}^{m}\left[\begin{array}{l} 3Sinh\left(\frac{2}{9}\right)-Sinh\left(\frac{1+\tilde{i}^2_{A_K}(x_i)+\left(1-\tilde{i}_{A_K}(x_i)\right)^2}{8+\left(\sqrt{\tilde{i}_{A_K}(x_i)}+\sqrt{1-\tilde{i}_{A_K}(x_i)}\right)^4}\right)-\left(\frac{2+\tilde{\mu}_{A_K}(x_i)+f_{A_k}(x_i)}{3}\right)Sinh\left(\frac{1+\tilde{\mu}^2_{A_K}(x_i)+\tilde{f}^2_{AIK}(x_i)}{8+\left(\sqrt{\tilde{\mu}_{A_K}(x_i)}+\sqrt{f_{A_k}(x_i)}\right)^4}\right) \\ -\left(\frac{4-\tilde{\mu}_{A_K}(x_i)-f_{A_k}(x_i)}{3}\right)Sinh\left(\frac{1+\left(1-\tilde{\mu}_{A_K}(x_i)\right)^2+\left(1-f_{A_k}(x_i)\right)^2}{8+\left(\sqrt{1-\tilde{\mu}_{A_K}(x_i)}+\sqrt{1-f_{A_k}(x_i)}\right)^4}\right) \end{array}\right];$$
$$0 \le \tilde{\mu}_{A_K}(x_i), \tilde{i}_{A_K}(x_i), f_{A_k}(x_i) \le 1 \forall i = 1,2,...,m$$

The various single valued neutrosophic entropy values $R_N(A_K)\left(K=1,2,...,9\right)$ are computed employing **(1)** and the results are displayed in **Table 2 and 3.**

Step:- 6 Using Maximum Argument Principle, the range order of each friction stir processed parameter based upon the existing Deluca-Termini 'fuzzy-entropy' measure proposed

hyperbolic fuzzy entropy (HFE) and 'single-valued-neutrosophic-entropy' (HNE) measures are depicted as illustrated in fig.6(a-d).

Diagnosis Results

Table 2 Energy Interval Ranges and Modified Energy Interval Ranges of Parameters of FSP $A_K\,(K=1,2,...,9)$

Rotational-Speed (r.p.m)	Processing-Speed (mm/min.)	Processing-Parameters A_K	Energy-Interval Ranges $\left[\bar{\mu}_{P_K}(x_i),\bar{U}_{P_K}(x_i)\right]$	Modified-Energy Interval-Ranges $\left[\tilde{\mu}_{P_K}(x_i),\tilde{U}_{P_K}(x_i)\right]$
1400	30	A_1	$[-0.026, 0.027]$	$[0.00068,0.00073]$
1500	30	A_2	$[-0.117, -0.065]$	$[0.01369,0.00423]$
1600	30	A_3	$[-0.125, -0.052]$	$[0.01563,0.00270]$
1400	40	A_4	$[-0.017,0.020]$	$[0.00029,0.00040]$
1500	40	A_5	$[-0.015,0.017]$	$[0.00023,0.00029]$
1600	40	A_6	$[-0.026,0.028]$	$[0.00068,0.00078]$
1400	50	A_7	$[-0.017,0.019]$	$[0.00029,0.00036]$
1500	50	A_8	$[-0.019,0.022]$	$[0.00036,0.00048]$
1600	50	A_9	$[-0.027,0.027]$	$[0.00073,0.00073]$

Table 3 Range Order of Friction Stir Processed Parameters $A_K\,(K=1,2,...,9)$ Based Upon Existing DTE, Proposed HNE and HFE Measures

Parameters	Single Valued Neutrosophic Sets	DTE Values	Range Order	HFE Values	Range Order	HNE Values	Range Order
	$\left[\tilde{\mu}_{A_K}(x_i),\tilde{i}_{A_K}(x_i),\tilde{f}_{A_K}(x_i)\right]$	$H(A_K)$		$H_{FS}(A_K)$		$R_N(A_K)$	
A_1	[0.00068,0.00005,0.99927]	0.0081	4	0.1183	4	0.3530	4

A_2	[0.01369,0.00100,0.99578]	0.1044	2	0.1308	2	0.3731	2
A_3	[0.01563,0.01000,0.99730]	0.1161	1	0.1320	1	0.3819	1
A_4	[0.00029,0.00011,0.99960]	0.0038	7	0.1173	7	0.3515	7
A_5	[0.00023,0.00006,0.99971]	0.0031	9	0.1171	9	0.3507	9
A_6	[0.00068,0.00011,0.99922]	0.0081	4	0.1183	5	0.3526	5
A_7	[0.00026,0.00010,0.99964]	0.0035	8	0.1172	8	0.3512	8
A_8	[0.00036,0.00012,0.99952]	0.0046	6	0.1175	6	0.3520	6
A_9	[0.00073,0.00001,0.99927]	0.0086	3	0.1184	3	0.3534	3

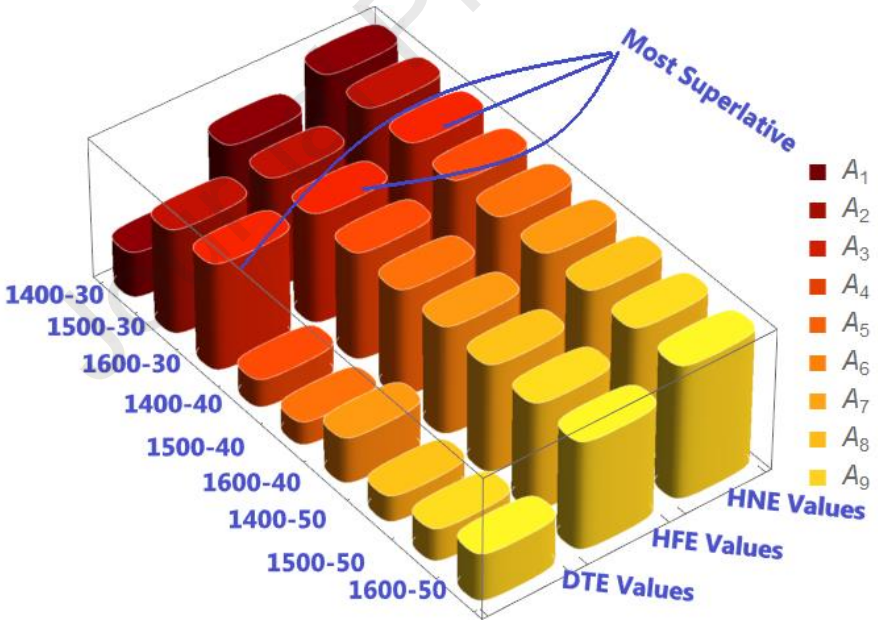

(a)

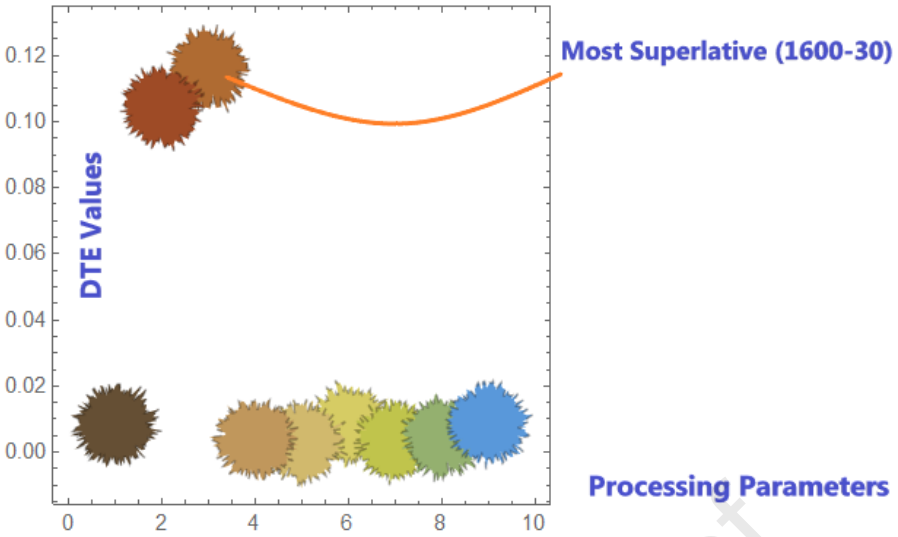

(b)

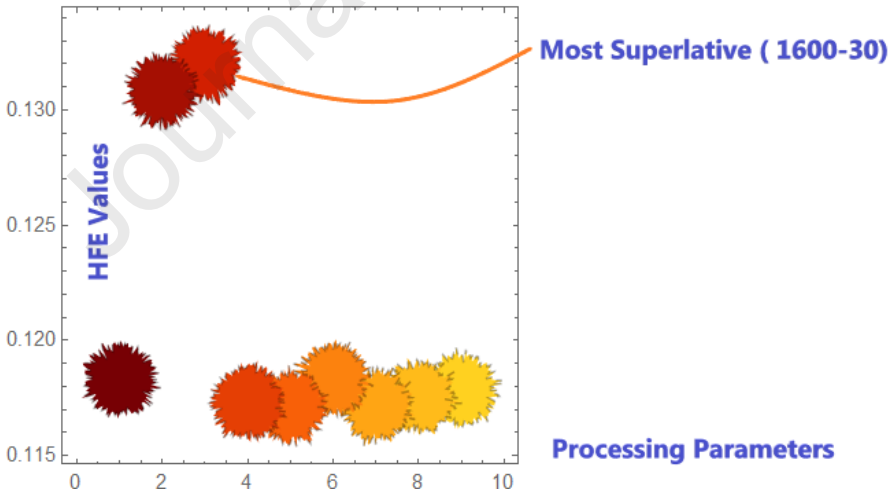

(c)

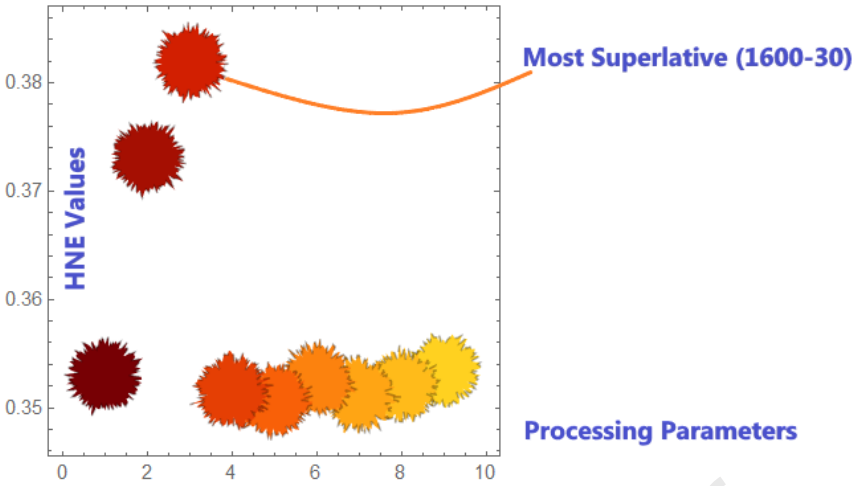

(d)

Fig.6 (a-d). Diagnosis results showing Energy Interval Ranges and Modified Energy Interval Ranges of Friction Stir Processed Parameters based upon Existing DTE, Proposed HNE and HFE Measures.

2.7. Vibration Analysis

For measuring the vibrations an accelerometer is mounted on the aluminum plate with a measure of 125 mm from the groove width's centre The signals are acquired by using accelerometer and further transferred to data acquisition-system from where signals are noted on the vibration measurement software and graphs are generated between the amplitude and time domain signals **[19-21]**. The mounting of the accelerometer on the fixture shown in Fig.7. After acquiring the data for amplitude and time domain, analysis of this data is performed on the MATLAB software and graphs are generated for Fast-Fourier Transform and various statistical parameters. The whole acquisition of the signal is carried for about 2.5 to 3 min.

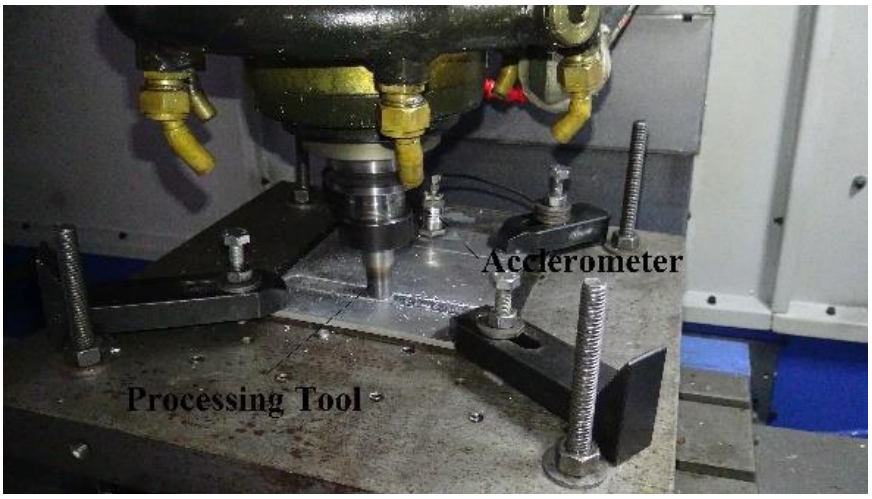

Fig.7. Mounting of Acclerometer on Plate.

The same procedure is followed for number of experiments under different rotational speeds and at different feed rate and finally computation is done for finding at which rotational speed and feed rate the vibration signals shows less randomness, because due to less vibrations the processing should be free from all kinds of defects and flaws.

2.8. Wear Rate

Pin-on-disc tribometer was assigned to test the 'wear-resistance' of the treated specimens. **[28-32]**. Specimens with the dimensions, as per ASTM G99 standards were prepared as shown in Fig.8(a), and Fig.8(b).

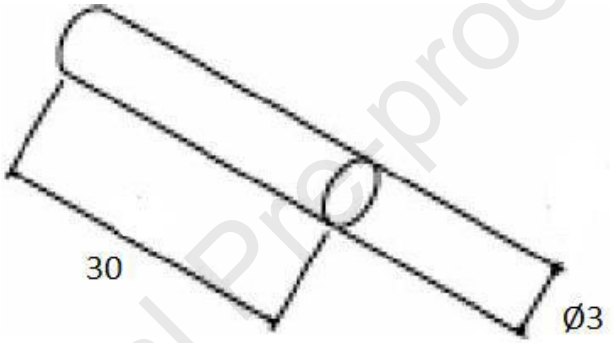

(a)

(b)

Fig.8. (a) Wear sample dimensions in mm; (b) Wear samples.

3. Results and Discussions:

3.1. FTT for Vibration-Analysis

Fast-Fourier Transform of the vibration signal were examined and found that, while processing under different 'rotational-speed' and 'feed-rate' the graphs are following a similar trend shown in Fig.9.

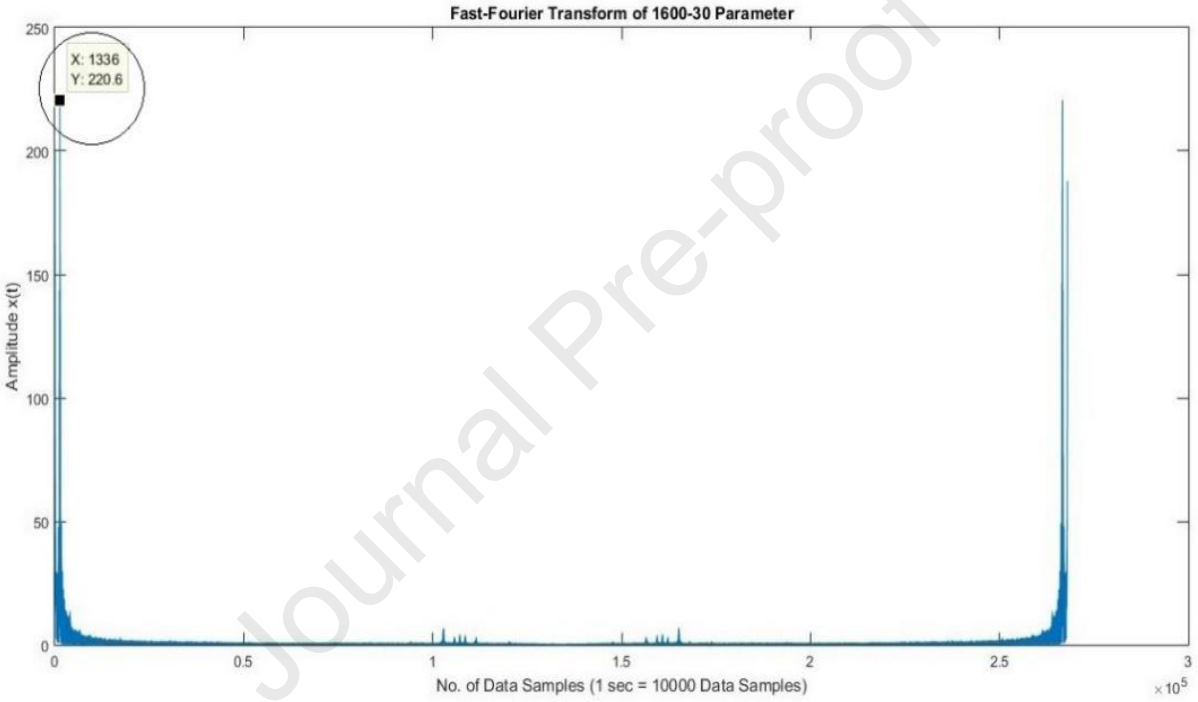

Fig.9. (a) FFT for 1600-30 Parameter; (b) Enlarge View of Isolated Peaks.

The randomness in the signal is higher at the starting of the process and at the completion of the process. This is due to the vibrations imparted in the system at the time of tool insertion and tool exit, because in the starting duration a high-speed steel tool rotating was inserted in the plate which is in steady condition so at that time of instant the FFT is showing higher randomness in the signal. In sometime the vibration becomes less because the continuous motion of the tool in the plate generates heat due to which the material gets softened and at that time of instant the vibration is less. Similarly, at the time of tool exit the vibrations are higher in each case of processing parameters.

3.2. Analysis of Statistical Parameters for Vibration Analysis

In this process there are certain statistical parameters are examined and the effect of each parameters on the vibration signal is investigated. The statistical analysis is presented in Table 4 for each individual processing parameter such as the feed rate 30, 40 and 50 mm/min. respectively.

Table 4. Statistical Parameters for Vibration Analysis

Statistical Parameter	Standard Deviation	Kurtosis	Shannon
1400-30	9.5295	7.44×10^{4}	2.11×10^{7}
1500-30	9.6023	7.84×10^{2}	9.64×10^{6}
1600-30	8.9076	2.01×10^{4}	4.26×10^{6}
1400-40	5.0713	1.35×10^{4}	2.75×10^{6}
1500-40	8.1556	5.41×10^{3}	1.96×10^{7}
1600-40	5.6011	1.33×10^{4}	1.05×10^{7}
1400-50	4.8432	-5.30×10^{3}	1.07×10^{7}
1500-50	4.4692	7.14×10^{4}	6.57×10^{6}
1600-50	4.9345	-1.54×10^{5}	5.33×10^{6}

In the above statistical analysis Shannon entropy was showing most significant results at different feed-rate and rotational-speed. The variation of Shannon values with respect to the constant ‘rotational-speed’ of 1600 rpm and increased ‘feed-rate’ from 30 to 50 mm/min. was illustrated in Fig.10(a)-(b).

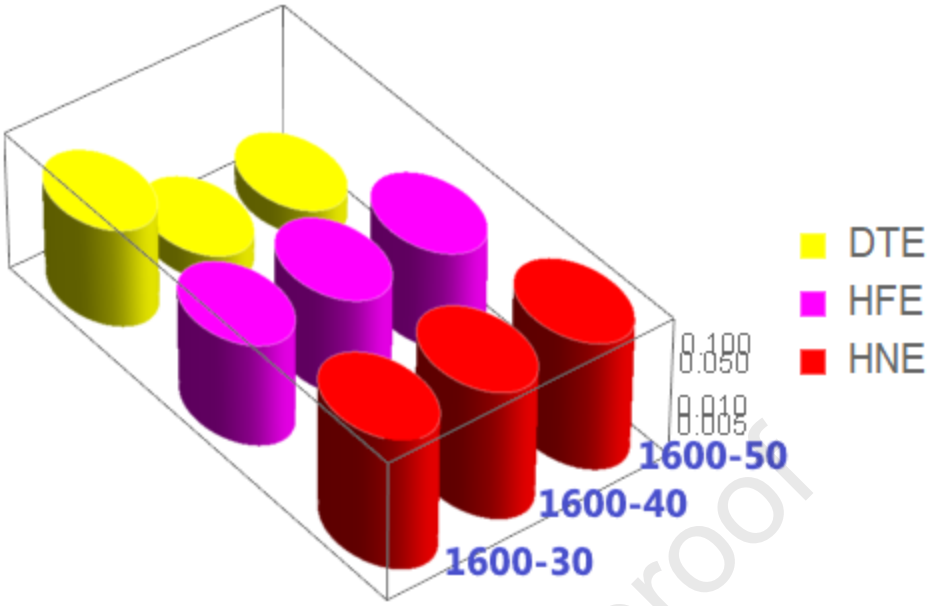

(a)

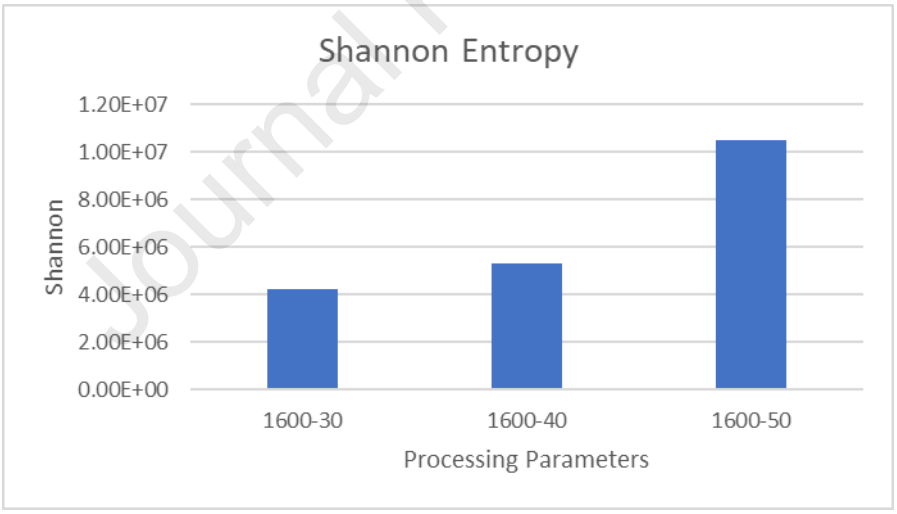

(b)

Fig.10(a-b). Shannon at constant-rotational-speed of 1600 rpm.

It has been found that the randomness in the signal is high in the case of high feed-rate this is due to the tool motion which generates heat in the plate. At higher feed rate the heat generation was less. So, more metal-metal contact occurs between the plate material and the tool results in the larger amount of randomness in the signal. The variations in the parameters

presented that at 1600 speed and at 30 (mm/min.). The feed-rate the randomness in the signal was least.

3.3. Results of Wear-Rate

In Fig.11, the wear-rates of samples manufactured at various rotational-speeds were compared to those of the basic material. In comparison to the base-material, the samples generated with B_4C particles exhibit a better 'wear-resistance' trend with increasing 'rotational-speed', while the samples fabricated without B_4C incorporation show the reverse trend with rising rotational-speed.

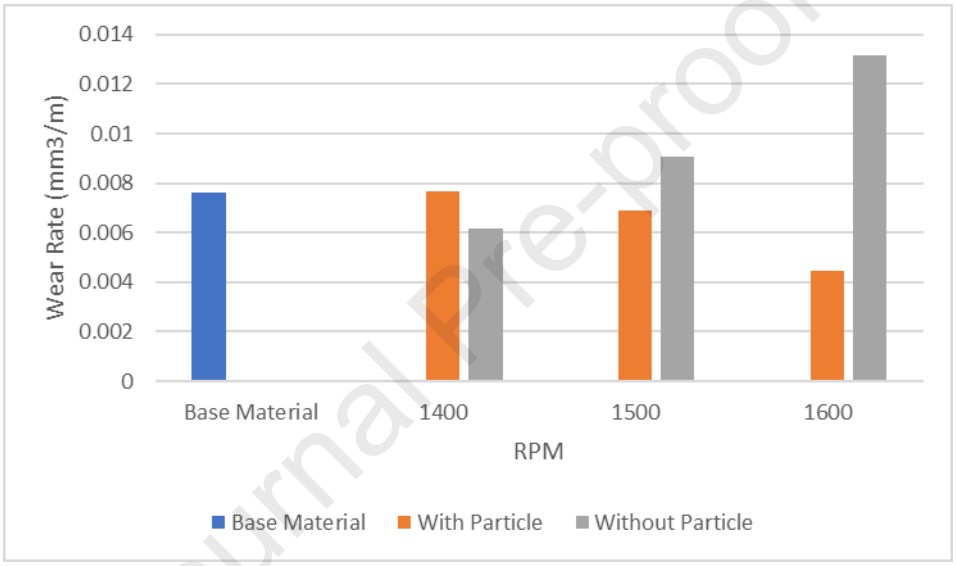

Fig.11. Comparison of wear rates (with and without particles) with base metal.

The MMC has greater wear resistance than FSPed and as received-alloy because the B_4C particle-distribution is more uniform, causing the particles to behave as load supporting elements and reducing the 'load' between the disc & the specimen-surface. The matrix alloy's 'fine-grain-size' decreases as 'rotating-speed' increases due to FSP. It has been established that the 'wear-rate' increases with increasing 'rotational-speed' because increased 'rotational-speed' increases heat-generation in the 'nugget zone', resulting in matrix alloy softening and increasing wear-rate [28-32]. Because the B_4C particles are not distributed uniformly in the matrix at lower 'rotational-speeds,' the hard ' B_4C particles' pulled out from the composite-pin and stacked over the steel-disk and start acting as a shield during the wear-process in Fig.11, the specimen manufactured at minimum 'rotational-speed' by assorted reinforcement-particles shows higher wear than the specimen fabricated without-particle incorporation. As a result,

more material wears out from the composite pin. Similar findings were found by Yuvaraj et al. [9] and Devaraju et al. [10] for Al5083- B_4C and Al-SiC/Gr and Al-SiC/Al2O3 at varied rotational speeds. The wear resistance of the MMC is improved when compared to the base material and FSPed alloy due to the addition of hard-ceramic particles, which improves hardness and matrix refinement.

3.4. Results of COF

The Fig.12, represents the variation of COF with respect to time for the samples-fabricated at different 'rotational-speed' and found that with increasing the 'rotational-speed' the COF increases.

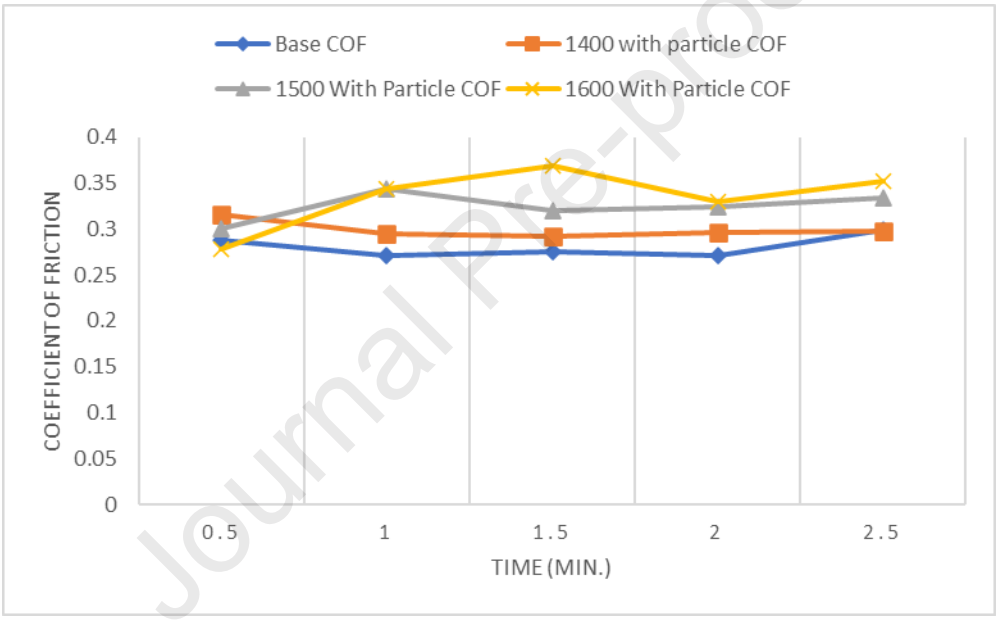

Fig.12. COF with particle comparison with base-metal.

The specimens fabricated at 1600 'rotational-speed' exhibits maximum COF, while the same has been found to have the highest 'wear-resistance' due to a higher volume of B_4C-particle-distribution. It was concluded that B_4C ceramic-particles get reinforced in the matrix that outcomes in more COF. H.G. Rana et al. **[11]** for Al7075- B_4C fabrication also investigated the same kind of result. The comparable outcomes have been reported to evident the enhancement of the electrical and mechanical capabilities of this material, Siddharthan et al. (2022) have developed "Aluminium metal-matrix Composites" (Al-MMC) [33]. This was accomplished by selecting four compositions. Al 8011 is available in four different graphite content variations: 2 percent, 4 percent, and 6 percent. Due to its simplicity, low cost, and

potential for large-scale manufacturing, stir casting was chosen among the various manufacture processes accessible for the creation of AMMC. A number of tests including Ductile, Rockwell, Impact, wear, optical microscopy, and electrical conductivity were carried out on the pre-arranged composites, and the results were compared to an unreinforced material. The reinforced material exhibited superior elasticity than that of the unreinforced material according to the Tensile test. A rise in hardness values can be observed as more particles are built up. Adding reinforcements and conducting an electrical conductivity test on the specimen improved its wear properties according to the tribological concentration. Studies unequivocally demonstrated that the addition of graphite enhanced the supported aluminum composite's mechanical, electrical, and tribological properties. The microstructure analysis supports the matrix's reinforcement's uniform scattering [33]. Another study proved that the metal matrix composites (MMC) based on self-lubricating aluminium were being explored to compare the effects of graphene and graphite as reinforcement on the material characteristics, wear, and friction [34]. With the inclusion of graphene, there was a noticeable improvement in mechanical properties as well as friction and wear performance. According to statistical research, aluminium MMCs with a higher percentage of graphite could provide friction and wear performance equivalent to that of graphene-reinforced MMCs made of significantly less graphene. In order to forecast the wear rate and coefficient of friction (COF) of aluminum-graphene MMCs, five machine learning (ML) regression models were created. According to ML research, the loading circumstances, hardness, and weight percent of graphene had the biggest effects on the wear and friction of aluminum-graphene [34].

Additionally, industries are advancing quickly, necessitating the creation of innovative materials with certain properties [35]. For metals used in maritime applications, automotive applications, the aerospace sector, etc., qualities like hardness, wear resistance, flexural strength, and corrosion resistance are particularly important. The aluminium metal matrix composites (AMMCs) are attractive materials that satisfy industry standards. The primary goal of this study is the creation of materials with the most essential qualities that may be used in stir casting to create parts for EDM applications in the automotive, aerospace, and marine industries. Al6101 is employed as the matrix material in this study, along with boron carbide (B4C), carbon nanotubes (CNT), and selenium (Se), all of which have fixed weight ratios of 0.7 percent, 0.15 percent, and 0.7%, respectively, as reinforcing components. Additionally, stir casting is used to create five different combinations of reinforcing materials for the Al6101-Se/B4C/CNT composite samples (S1, S2, S3, S4, S5). The findings of further

research into features, including hardness, corrosion resistance, wear resistance, flexural strength, and electrical conductivity, revealed that the addition of reinforcements improves these properties [35]. Another study has utilised a tungsten inert gas welding, where the aluminium metal matrix composites with different amounts of SiC reinforcement were being fused/joined [36]. The welding settings remained the same for every aspect of the specimen. Thermal ageing was used to reach the age-hardening peak for the welded composites. Microstructural differences between aged and non-age hardened composites are highly significant, including grain boundary fractions, misorientation, and energy storage. The mechanical performance of the welded composites underwent identical modifications that revealed these variances in the microstructure. Microstructure after age revealed improved grain size and preferred orientation. The hardness of SiC has been shown to rise at distinct rates with rising SiC concentrations. This indicates that hardness is clearly a function of energy storage and strength of misorientation. Measurements of EBSD indicate that age-hardening caused a rearrangement in dislocation substructures accompanied by the precipitation of Mg2Si or a rise in SiC content. The weld metal dynamically recovers, increasing hardness. Recovery exhibited a predominance of precipitation strengthening in comparison to the annihilation of dislocations due to increased tensile strength with decreasing misorientation. The current work will explore the effects of adding SiC to aluminium metal matrix composites on their welded microstructural properties. This will enable us to understand how these changes influence the observed mechanical behavior of the welded joints. Research has shown that both the distribution and average values of misorientation influence the strength of the approach [36]. Relative pressures have a massive impact on how well materials function under use [37]. The introduction of high-amplitude and large-depth compressive residual stresses is achieved by laser shock peening, a technique that produces residual stresses based on the process. Surface residual stresses resulting from LSP following single shots and overlapping shots. By employing the 10 J, 20 J, 30 J, and 40 J of laser energy to introduce single-shot LSP, an average surface residual stresses were being introduced that has been ranged from 126.7%, 129%, 85.7 %, and 69.2%. Each shot with an energy of 20 J twice was fired against the test surface several times; the maximum effective compressive stress measured was 266.7 MPa. Surface residual stress decreased from 266.7 MPa to 215.3 MPa, then to 212.7 MPa after being subjected to 10,000 and 100,000 fatigue cycles. Thermal loads also caused relaxation, and after 50 hours of storage at 100 °C, the tension dropped from 266.7 MPa to 129.3 MPa. Furthermore, the SiC/2009Al composite was simulated to demonstrate its response to the LSP process. This has showed that SiC particles

at the peening surface produced the greatest tensile stress and reverse plastic deformation. An empirical and numeric combination study is being conducted in an attempt to provide a comprehensive understanding of residual stress [37].

4. Conclusions

In the research work, the specific wear rate under dry conditions and vibrational analysis was carried out by using novel hyperbolic fuzzy entropy (HFE) and single valued neutrosophic entropy (NFE) based methodology. The following conclusions are drawn for AA7075/ B_4C aluminum composite, and optimized result were obtained at feed-rate of 30 mm/min and tool-rotational speed of 1600 rpm giving best surface finish and producing negligible processing defects as detailed follows:

a. The base material has a higher wear-rate than the MMC samples. The sample made at 1600 rpm with hard B_4C particles shows the least-wear of all the samples evaluated. On the other hand, sample made at 1400 rpm without B_4C particles shows the least wear of all the specimens evaluated. In comparison to the base material, the samples generated by integrating B_4C particles exhibit a better wear-resistance trend with increasing rotational-speed, while the samples fabricated without B_4C incorporation show the opposite tendency with rising rotational-speed.

b. The sample fabricated at 1600 speed display higher COF.

c. FFT of the vibration-signal shows that, while processing under different RPM and feed rate the graphs are following a similar trend. The variations in the vibration signal of 30 mm/min feed rate shows that at 1600 rpm the randomness in the signal was less. It means 30 mm/min feed-rate and 1600 rotational-speed are the most optimum-parameters for friction stir processing of AA7075 integrated with B_4C particles.

d. Aluminium metal matrix composites with high specific stiffness and high strength could be used in long-term application in which saving weight is an important feature, such applications include robots, high speed machinery, high-speed rotating shafts, and automotive engine and brake parts.

Declaration of conflict of Interest:

The authors declare that they have no conflict of interest with respect to the research, authorship, and/or publication of this article.

Funding:

The authors doesn't receive any research fund or grant from any organization.

Ethical approval:

This article does not contain any studies with human participants or animals performed by the author.

References

1. https://en.wikipedia.org/wiki/Friction_stir_processing.
2. https://en.wikipedia.org/wiki.sintering
3. http://www.sapagroup.com/en/sapa-profilyas/aluminum/aluminum-alloys
4. A. Shafiei-Zarghani et al. (2011), "Wear assessment of Al/Al2O3 nano-composite surface layer produced using friction stir processing", International Journal on the Science and Technology of Lubrication and Wear, Vol. no 270, pp 403-412.
5. Mohsen Barmouz et al. (2011), "On the role of processing parameters in producing Cu/SiC metal matrix composites via friction stir processing: Investigating microstructure, microhardness, wear and tensile behaviour", Material Characterization, Vol. no 62, pp 108-117.
6. S.A. Alidokht et al. (2011), "Microstructure and tribological performance of an aluminium alloy-based hybrid composite produced by friction stir processing", Materials and Design, Vol. no 32, pp 2727-2733.
7. S. Amini et al. (2014), "Study of ultrasonic vibrations' effect on friction stir welding".
8. ELISEEV Alexander et al. (2016), "Effect of Ultrasonic Application during Friction Stir Welding on Microstructure and Properties of AA2024 Fixed Joints", Key Engineering Materials, Vol. no 683, pp 227-231.
9. Narayan Yuvaraj et al. (2015), "Fabrication of Al5083/ B_4C surface composite by friction stir processing and its tribological characterization", Journal of Material Research and Technology.
10. A. Devaraju et al. (2013) "Influence of addition of Grp/Al2O3p with SiCp on wear properties of aluminium alloy 6061-T6 hybrid composites via friction stir processing", Transactions of Nonferrous Metals Society of China, Vol. no 23, pp 1275-1280.

11. H.G. Rana et al. (2016), "Fabrication of Al7075 / B_4C surface composite by novel Friction Stir Processing (FSP) and investigation on wear Properties", Procedia Technology, Vol. no 23, pp 519-328.
12. Sharma, H., Kumar, K., Kumar, R., & Gulati, P. (2018). A Study of Vibration and Wear Resistance of Friction Stir Processed Metal Matrix Composite. Materials Today: Proceedings, 5(14), 28354-28363.
13. Sharma, H., Tiwari, S. K., Deepmala, K., & Gupta, A. Investigation of mechanical and tribological properties of the Al7075- B_4C composite fabricated by friction stir processing.
14. Anvari, Razieh & Karimzadeh, Fathallah & Enayati, Mohammad Hossein. (2013). Wear characteristics of Al–Cr–O surface nano-composite layer fabricated on Al6061 plate by friction stir processing. Wear. 304. 144–151. 10.1016/j.wear.2013.03.014.
15. Sathiskumar, R. & Murugan, N. & Dinaharan, Isaac & Santhiyagu, Vijay. (2013). Characterization of boron carbide particulate reinforced in situ copper surface composites synthesized using friction stir processing. Materials Characterization. 84. 16-27. 10.1016/j.matchar.2013.07.001.
16. Sathiskumar, R. & Murugan, N. & Dinaharan, Isaac & Santhiyagu, Vijay. (2013). Prediction of mechanical and wear properties of copper surface composites fabricated using friction stir processing. Materials & design. 55. 10.1016/j.matdes.2013.09.053.
17. Rajwinder Singh Gill, Partap Singh Samra, Amresh Kumar, (2022), Effect of different types of reinforcement on tribological properties of aluminium metal matrix composites (MMCs) – A review of recent studies, material today proceedings, 56, 3094-310. 10.1016/j.matpr.2021.12.211.
18. Akramifard, Hamid & Shamanian, Morteza & Sabbaghian, Mahdi & Esmailzadeh, Mojtaba. (2013). Microstructure and mechanical properties of Cu/SiC metal matrix composite fabricated via friction stir processing. Materials and Design. 54. 838-844. 10.1016/j.matdes.2013.08.107.
19. Ikumapayi, Omolayo & Akinlabi, Esther. (2019). Experimental Data on Surface Roughness and Force Feedback Analysis in Friction Stir Processed AA7075 -T651 Aluminium Metal Composites. Data in Brief. 23. 10.1016/j.dib.2019.103710.

20. Zadeh, L.A. (1965) Fuzzy Sets. Information Control, 8, 338-353. http://dx.doi.org/10.1016/S0019-9958(65)90241-X.

21. Smarandache. F. (1998), "Neutrosophy: neutrosophic probability, set and logic. American Research Press Rehoboth.". DE, USA.

22. Moslem Paidar, Olatunji Oladimeji Ojo, Akbar Heidarzadeh, and Hamid Reza Ezatpour, Influence of multi-pass FSP on the microstructure, mechanical properties and tribological characterization of Al/B4C composite fabricated by accumulative roll bonding (ARB), Surface and Coatings Technology, 2019, 361, Pages 159-169. https://doi.org/10.1016/j.surfcoat.2019.01.043.

23. Alireza Moradi Faradonbeh, Morteza Shamanian, Hossein Edris, Moslem Paidar and Yahya Bozkurt, Friction Stir Welding of Al-B4C Composite Fabricated by Accumulative Roll Bonding: Evaluation of Microstructure and Mechanical Behavior, Journal of Materials Engineering and Performance, 2018, 27, Pages 835-846. https://doi.org/10.1007/s11665-018-3131-2.

24. Moslem Paidar, Dmitry Bokov, Sadok Mehrez, Olatunji Oladimeji Ojo, Vaira Vignesh Ramalingam, Shabbir Memon, Improvement of mechanical and wear behavior by the development of a new tool for the friction stir processing of Mg/B4C composite, Surface and Coatings Technology, 2021, 426, https://doi.org/10.1016/j.surfcoat.2021.127797.

25. Bhandari D. and Pal N.R. (1993), "Some new information measures for fuzzy sets, Information Sciences, 67, 209-226. https://doi.org/10.1016/0020-0255(93)90073-U.

26. A. De Luca, S. Termini, A definition of a non-probabilistic entropy in the setting of fuzzy sets theory, Information and Control, 20 (4), 1972, pp. 301-312, https://doi.org/10.1016/S0019-9958(72)90199-4.

27. Dubois, D., and Prade, H., Fundamentals of Fuzzy Sets, Kluwer Academic Publishers, Boston (2000). 10.1007/978-1-4615-4429-6.

28. Jeon, Chi-Hoon & Jeong, Yong-Ha & Seo, Jeong-Jin & Tien, Huynh & Hong, Sung-Tae & Yum, Young-Jin & Hur, Seung & Lee, Kwang-Jin. (2014). Material properties of graphene/aluminum metal matrix composites fabricated by friction stir processing. International Journal of Precision Engineering and Manufacturing. 15. 1235-1239. 10.1007/s12541-014-0462-2.

29. Zhao, Yong & Huang, Xiaolu & Li, Qiming & Huang, Jian & Yan, Keng. (2015). Effect of friction stir processing with B_4C particles on the microstructure and mechanical properties of 6061 aluminum alloy. The International Journal of Advanced Manufacturing Technology. 78. 10.1007/s00170-014-6748-9.

30. Shi, Lei & Wu, C.S. & Liu, X.. (2015). Modeling the effects of ultrasonic vibration on friction stir welding. Journal of Materials Processing Technology. 222. 10.1016/j.jmatprotec.2015.03.002.

31. Mazaheri, Y., Heidarpour, A., Jalilvand, M.M. et al. Effect of Friction Stir Processing on the Microhardness, Wear and Corrosion Behavior of Al6061 and Al6061/SiO2 Nanocomposites. J. of Materi Eng and Perform 28, 4826–4837 (2019). https://doi.org/10.1007/s11665-019-04260-3.

32. M.M. Jalilvand, Y. Mazaheri, A. Heidarpour, and M. Roknian, Development of A356/Al2O3 + SiO2 Surface Hybrid Nanocomposite by Friction Stir Processing, Surf. Coat. Technol., 2019, 360, p 121–132. https://doi.org/10.1016/j.surfcoat.2018.12.126.

33. B.Siddharthan, A. Kumaravel, and Jones Praveen J, Mechanical and electrical characterization of aluminium alloy metal matrix composites reinforced with graphite, Material today proceeding, 2022, https://doi.org/10.1016/j.matpr.2022.05.228.

34. Md SyamHasan, TienWong, Pradeep K.Rohatgi, Michael Nosonovsk, Analysis of the friction and wear of graphene reinforced aluminum metal matrix composites using machine learning models, 2022, 170, https://doi.org/10.1016/j.triboint.2022.107527

35. Hari Prasad M. Venkata Ramaiah P, Fabrication and characterization of Aluminum 6101-Selenium/boron carbide /carbon nanotubes metal matrix nano composites, Material today proceeding, 2022, https://doi.org/10.1016/j.matpr.2022.05.271

36. Jayashree PK, Gowrishankar MC, Sathyashankara Sharma, Raviraj Shetty,PavanHiremath, and Manjunath Shettar, The effect of SiC content in aluminum-based metal matrix composites on the microstructure and mechanical properties of welded joints, Journal of Materials Research and Technology, 2021, 12, https://doi.org/10.1016/j.jmrt.2021.04.015.

37. Rujian Sun, Ziwen Cao, Zhigang Che, Hepeng Zhang, Shikun Zou, Junfeng Wu, and Wei Guo, A combined experimental-numerical study of residual stress and its relaxation on laser shock peened SiC particle-reinforced 2009 aluminum metal matrix composites, 2022, 430, https://doi.org/10.1016/j.surfcoat.2021.127988.

Declaration of interests:

✓ The authors declare that they have no known competing financial interests or personal relationships that could have appeared to influence the work reported in this paper.

☐ The authors declare the following financial interests/personal relationships which may be considered as potential competing interests:

The authors declare that they have no conflict of interest with respect to the research, authorship, and/or publication of this article. The authors don't receive any research fund or grant from any organization. This article does not contain any studies with human participants or animals performed by the author.

Szymon Wojciechowski
First Corresponding Author
Faculty of Mechanical Engineering and Management,
Poznan University of Technology,
Poznan, 60-965, Poland.
E-Mail: sjwojciechowski@o2.pl

Shubham Sharma
Second Corresponding Author
Department of Mechanical Engineering,
IK Gujral Punjab Technical University,
Main Campus-Kapurthala, 144603, Punjab, India.
E-Mail: shubham543sharma@gmail.com
shubhamsharmacsirclri@gmail.com